

**WASHINGTON UNIVERSITY IN ST. LOUIS
SCHOOL OF ENGINEERING AND APPLIED SCIENCE
DEPARTMENT OF MECHANICAL, AEROSPACE & STRUCTURAL
ENGINEERING**

**IN SITU WIRELESS SENSING FOR DISTRIBUTED
STRUCTURAL HEALTH MONITORING**

by

Nestor E. Castaneda

Prepared under the direction of Professor S. J. Dyke

**Thesis presented to the School of Engineering and Applied Science of
Washington University in St. Louis in partial fulfillment of the
requirements of the degree of
MASTER OF SCIENCE
December 2008
Saint Louis, Missouri**

WASHINGTON UNIVERSITY IN ST. LOUIS
SCHOOL OF ENGINEERING AND APPLIED SCIENCE
DEPARTMENT OF MECHANICAL, AEROSPACE & STRUCTURAL
ENGINEERING

ABSTRACT

IN SITU WIRELESS SENSING FOR DISTRIBUTED
STRUCTURAL HEALTH MONITORING

by

Nestor E. Castaneda

ADVISOR: Professor S. J. Dyke

December 2008

Saint Louis, Missouri

Wireless sensors have become a promising and novel solution for structural health monitoring (SHM) applications during recent times. Due to their low implementation costs and embedded computational capacities, monitoring of structural condition at unprecedented spatial resolution is a near-term possibility. However, distributed processing techniques capable of detecting damage must be co-implemented in parallel with power and communication requirements to expand their applicability. In this work, a distributed damage detection system is proposed and experimentally validated using a wireless sensor network deployed on two laboratory structures. On-board processing capabilities of the wireless nodes are exploited to significantly reduce the communication load and power consumption. The Damage Location Assurance Criterion (DLAC) is adopted as the damage detection technique. Processing of the raw data is conducted locally at the sensor level, and a reduced data set is transmitted to the base station for decision-making. The results indicate that this distributed implementation can be used to successfully detect and localize regions of damage in a structure.

copyright by
Nestor E. Castaneda
2008

To the most important people in my life: my beloved parents, sister and wife

Contents

List of Tables	vii
List of Figures	viii
Acknowledgements	x
1. Introduction.....	1
1.1 The importance of distributed techniques in SHM	6
1.2 Overview	12
2. Distributed Damage Detection System Implementation	14
2.1 Overview	14
2.2 Data Acquisition	16
2.2.1 Sensor Board	16
2.3 Data Processing	20
2.3.1 Fast Fourier Transform	20
2.3.2 Power Spectral Density	21
2.3.3 Curve Fitting Technique	23
2.3.4 iMote2 Platform	25
2.4 Data Transmission	26
2.4.1 Latency and Data Reduction Analysis.....	28
2.4.2 Energy Usage Analysis	29
2.5 Damage Localization Algorithm	29
2.5.1 Equation Solver Routine.....	30

2.5.2 Damage Location Assurance Criterion (DLAC)	31
2.6 Description of User Interface	34
2.7 Summary	35
3. Cantilevered Beam Experiment	36
3.1 Experimental Setup	36
3.2 Numerical Model	38
3.3 Experimental Results	39
3.4 Summary	46
4. Truss Structure Experiment.....	47
4.1 Experimental Setup	48
4.2 Numerical Model	50
4.3 Experimental Results	51
4.4 Off-Line Experimental Results.....	54
4.5 Additional Numerical Studies	58
4.6 Summary	62
5. Conclusions and Future Work	63
References	68
Vita	74

Tables

Table 1.1: Academic wireless sensor platforms	3
Table 1.2: Commercial wireless sensor platforms.....	4
Table 2.1: Accelerometer user specified sampling rates	18
Table 2.2: iMote2 Main Board Properties	26
Table 2.3: Latency Analysis Table	28
Table 3.1: Analytical natural frequencies (Hz).....	38
Table 3.2: Experimental healthy natural frequencies (Hz)	40
Table 4.1: Analytical natural frequencies (Hz).....	51
Table 4.2: Experimental healthy natural frequencies (Hz)	52
Table 4.3: Identified natural frequencies (Hz)	54
Table 4.4: Analytical natural frequencies (Hz).....	55

Figures

Figure 1.1: Wireless sensor nodes deployed on one of the beam girders.....	7
Figure 1.2: Wireless sensor setup (after Gangone et al, 2007)	8
Figure 1.3: Layout of nodes deployed on The Golden Gate Bridge.....	8
Figure 1.4: Panoramic view of road test deployments (after Pei et al., 2008)	9
Figure 1.5: Examples of SHM implementations under hierarchical architectures	11
Figure 2.1: Flow chart of implementation	15
Figure 2.2: Top and bottom view of basic sensor board.....	18
Figure 2.3: Wireless sensor time history record	19
Figure 2.4: Corresponding Power Spectral Density Function	22
Figure 2.5: Power Spectral Density and Curve Fitting.....	25
Figure 2.6: Top and bottom view of iMote2 main board	26
Figure 2.7: Correlation Factors calculated with the DLAC.....	33
Figure 2.8: User-interface	34
Figure 3.1: Diagram of cantilever beam test structure	37
Figure 3.2: View of cantilever beam experiment	37
Figure 3.3: View of sensor distribution on cantilever beam experiment.....	38
Figure 3.4: Cantilevered beam finite element model.....	39
Figure 3.5: WS2 acceleration record and corresponding PSD under damage scenario D1	41
Figure 3.6: WS4 acceleration record and corresponding PSD under damage scenario D2	41
Figure 3.7: WS1 acceleration record and corresponding PSD under damage scenario D3	42

Figure 3.8: DLAC results for element position # 5	43
Figure 3.9: DLAC results for element position # 10	44
Figure 3.10: DLAC results for element position # 14	45
Figure 4.1: 3D truss test structure.....	47
Figure 4.2: Truss experiment setup	48
Figure 4.3: Truss experiment setup	49
Figure 4.4: Two views of the sensor setup	49
Figure 4.5: Truss finite element model.....	50
Figure 4.6: View of Magnetic Shaker.....	52
Figure 4.7: DLAC results for truss bay # 3	53
Figure 4.8: Truss finite element model.....	55
Figure 4.9: DLAC results for truss bay # 3 under 25 % of area section Reduction.....	56
Figure 4.10: DLAC results for truss bay # 3 under 50 % of area section Reduction.....	57
Figure 4.11: Numerical simulation setup.....	58
Figure 4.12: Typical acceleration time history and corresponding PSD Function	59
Figure 4.13: DLAC results for truss bay #6 under 25% and 50 % of area section Reduction.....	60
Figure 4.14: DLAC results for truss bay #11 under 25% and 50 % of area section Reduction.....	61

Acknowledgments

I would like to express my sincere gratitude to my advisor, Dr. Shirley Dyke, for her constant support and patience during the development of my studies. Without her advice this work would not have been a reality.

I would also like to thank Dr. Chenyang Lu for his advice and my computer science graduate student colleagues Fei Sun, Cheng-Lian Fok and Greg Hackmann for their constant support in the use of the sensors and the software development efforts.

My sincere gratitude is dedicated to my fellow graduate students in the Structural Control and Earthquake Engineering Laboratory at Washington University in St. Louis. Their support and company will be always much appreciated.

Special thanks to Professor Bill Spencer and graduate student colleague, Shin-Ae Jang, for the use of and assistance with the experimental truss located at the Smart Structure Technology Laboratory (SSTL) at the University of Illinois at Urbana-Champaign.

Funding for this research is provided in part by the National Science Foundation; grant NSF NeTS-NOSS Grant (CNS-0627126), NSF CRI Grant (CNS-0708460), and by Washington University in St. Louis.

Nestor E. Castaneda

Chapter 1

Introduction

Structural health monitoring (SHM) is an exciting research field in which damage detection strategies are implemented to examine the serviceability condition of structures. The measured spatial and quantitative information from continuously monitoring the structure is used then to predict the performance of its lifecycle. Although structural health condition assessment is not a new topic, most of the research efforts in developing damage detection systems for civil, aerospace and mechanical SHM applications have taken place during the last fifteen years involving different branches of engineering. Damage detection algorithms typically use the dynamic behavior of the structure, commonly as raw acceleration or strain measurements, to detect potential structural damage zones. Because, the structural damage is initially evidenced as localized changes in the material and geometrical properties of the structure, structural response measurement is accomplished through the use of a sensor network homogeneously distributed over the entire structure. However, to accurately capture the dynamic response and complexities present in the behaviors of a real structure, the deployment of a large number of sensors is usually required. As more sensors are used on the structure, the reliability of the measured response and quality of the damage information increases.

Traditionally, damage detection systems have been designed to operate using wired sensor networks with centralized methodologies, where the raw data is directly streamed and gathered in a base station for further analysis. However, the applicability of these wired sensor implementations is limited due to the high costs associated with installation and maintenance of the sensor network. Even in relatively large structures, such as short span bridges or small buildings, it may be necessary to install thousands of power and data transmission cables, making implementation expensive and challenging.

In recent years, wireless sensor networks (WSN) equipped with microprocessors have appeared as a novel alternative for damage detection systems. The interest in their use has expanded in the SHM community due to their potential to provide a lower cost solution to the damage detection problem at an unprecedented spatial granularity. The possibility of using large WSN deployments is now a reality (Liu and Tomizuka, 2003; Spencer, 2003; Lynch et al., 2002). Powered wireless sensor platforms, bearing micro-electro-mechanical systems (MEMS) and microprocessors, can perform damage detection tasks efficiently by taking advantage of both their on-board processing and wireless communication capabilities. Microprocessors are used to perform on-board digital signal processing, data aggregation and self-operative functions, while the wireless communication attributes are used to transmit minimal amounts of processed information back to a base station for additional analysis and decision making.

Initial research efforts to develop wireless sensor platforms for damage detection systems include Straser and Kiremidjian (Straser and Kiremidjian, 1996; Kiremidjian et al., 1997; Straser and Kiremidjian, 1998) who developed a unit consisting of a microprocessor, radio modem, data storage and batteries with the capacity to maintain waiting and operational modes to account for power consumption.

Lynch also reported that several academic and commercial wireless sensor platforms have been developed during the last decade (Lynch, 2004; Lynch and Loh, 2006). Some examples of the most meaningful research to develop sensors for academic uses based on commercial-off-the-shelf components are discussed by Mason (Mason et al., 1995); Bult (Bult et al., 1996); Agre (Agre et al., 1999); Aoki (Aoki et al., 2003); Basheer (Basheer et al., 2003); Kawahara (Kawahara et al., 2003); Kottapalli (Kottapalli et al., 2003); Shinozuka (Shinozuka, 2003); Wang (Wang et al., 2003); Casciati (Casciati et al., 2004); Sazonov (Sazonov et al., 2004); Farrar (Farrar et al., 2005) and Lynch (Lynch, 2006). Although, these efforts have improved the state-of-the-art in smart sensor technology, the progress was deficient due to the absence of coordination between the different sources of research.

Table 1.1 Academic wireless sensor platforms

	<i>Straser and Kiremidjian, (1998)</i>	<i>Kottapalli et al. (2003)</i>	<i>Lynch et al. (2003)</i>	<i>Aoki et al. (2003)</i>	<i>Wang et al. (2003)</i>	<i>Farrar et al. (2005)</i>
DATA ACQUISITION SYSTEM						
<i>A/D Resolution</i>	16-bit	8-bit	16-bit		12-bit	16-bit
<i>A/D Channels</i>	8	5	1		8	6
<i>Sampling Frequency</i>	240 Hz	20 MHz	100 kHz		>50 Hz	
MICROPROCESSOR AND RADIO SPECIFICATIONS						
<i>Processor</i>	<i>Motorola 68HC11</i>	<i>Microchip PIC16F73</i>	<i>Atmel AT90S8515 AVR / MPC555 PowerPC</i>	<i>Renesas H8/4069F</i>	<i>Analog Devices ADuC832</i>	<i>Intel Pentium/ Motorola</i>
<i>Clock Speed</i>	2.1 MHz	20 MHz	4 MHz / 20 MHz	20 MHz		120/233 MHz
<i>Program Memory</i>	16 kB	4 kB	8kB / 26 kB	128 kB	62 kB	256 MB
<i>Data Memory</i>	32 kB	192 kB	512 kB / 448 kB	2 Mb	2 kB	Compact Flash
<i>Radio</i>	<i>Proxim ProxLink</i>	<i>BlueChip RBF915</i>	<i>Proxim RangeLan2</i>	<i>Realtek RTL-8019AS</i>	<i>Linx Technologies</i>	<i>Motorola neuRFon</i>
<i>Power Source</i>	<i>Battery (9 V)</i>	<i>Battery (9 V)</i>	<i>Battery (9 V)</i>		<i>Battery</i>	

In contrast, commercial smart sensor platforms offer users the technical expertise of the manufacturer and the opportunity to exploit an open hardware/software research platform. That is the case for the Mote wireless sensor platform, initially developed at the University of California-Berkeley and later commercialized by Crossbow (Crossbow Technologies, 2007). The Mote is an open source wireless sensor platform which enables users to customize the hardware and software based on their application (TinyOS, <http://www.tinyos.net/>). The mote has been under development since 1990 with its first “COTS Dust” (Hollar, 2000) and second “Rene” platform generation released in 1999.

The third generation, the “Mica mote,” with an improved memory capacity and faster microprocessor was released in 2001 (Hill and Culler, 2002). Successive improvements in the Mica mote platform resulted in the Mica2, Mica2dot and MicaZ.

Table 1.2 Commercial wireless sensor platforms

	<i>Rene</i> (1999)	<i>MICA</i> (2001)	<i>MICA2</i> (2003)	<i>Intel iMote</i> (2003)	<i>MicroStrain</i> (2003)
DATA ACQUISITION SYSTEM					
<i>A/D Resolution</i>	10-bit	10-bit	10-bit		12-bit
<i>A/D Channels</i>	8	8	8		8
<i>Sampling Frequency</i>	1 KHz	1 KHz	1 KHz		1.7 KHz
MICROPROCESSOR AND RADIO SPECIFICATIONS					
<i>Processor</i>	<i>Atmel</i> <i>Atmega</i> 163L	<i>Atmel</i> <i>ATmega</i> 103L	<i>Atmel</i> <i>ATmega</i> 128L	<i>Zeevo</i> <i>ARM7TDMI</i>	<i>MicroChip</i> <i>PIC16F877</i>
<i>Clock Speed</i>	4 Mhz	4 Mhz	7.383 Mhz	12 Mhz	
<i>Program Memory</i>	16 kB	128 kB	128 kB	64 kB	
<i>Data Memory</i>	32 kB	512 kB	512 kB	512 kB	2 MB
<i>Radio</i>	<i>TR100</i>	<i>TR100</i>	<i>Chipcon</i> <i>CC1000</i>	<i>Wireless BT</i> <i>Zeevo</i>	<i>RF Monolithics</i> <i>DR-3000-1</i>
<i>Power Source</i>	<i>Battery</i> (3 V)	<i>Battery</i> (3 V)	<i>Coin Cell</i>	<i>Battery</i>	<i>Battery</i> (3.6 V)

Close collaboration between the University of California-Berkeley and the Intel Research Berkeley Laboratory yielded the next generation of Mote platform called the “iMote” (Kling, 2003). The iMote has a modular construction which allows sensing interfaces interact by separated with the iMote circuit board. The iMote has a 32-bit ARM7TDMI microprocessor capable to operate at 12 MHz with 64 kB of RAM, 512 of ROM and integrated 2.4 GHz Zeevo Bluetooth radio.

In 2005, Intel also released the Intel *iMote2* (Adler et al., 2005) as an advanced wireless sensor platform which offers adequate processing and communication resources. Although a number of platforms have been developed, the Intel *iMote2* has emerged as the most appropriate for civil infrastructure monitoring under intensive conditions due to the on-board processing capabilities (Nagayama et al., 2006; Nagayama, 2007). The Intel *iMote2*'s compact size, implemented with interface connectors to interact with sensor

and battery boards, has made it a suitable platform for damage detection applications where long term operating conditions are required. Moreover, researchers have developed services for this platform that are now publicly available (Rice et al., 2008; The Illinois SHM Services Toolkit, 2008). Based on its computational advantages and successful previous research experiences, the Intel *iMote2* platform is selected for this study. *iMote2*'s main features are described in Chapter 2.

Many other companies have also dedicated efforts to develop smart sensor platforms for various applications. Companies such as Dust Networks (Dust Networks, <http://www.dust-inc.com>), Microstrain (MicroStrain Inc., <http://www.microstrain.com>), Millennial Net (Millennial Net, <http://www.millennial.net>), Sensametrics (Sensametrics, <http://www.sensametrics.com>) and Sensicast Systems (Sensicast Systems, <http://www.sensicast.net>) have released their own hardware and software versions with available technical support. Clayton also provided a summary of the most meaningful commercial and academic wireless sensor platforms developed from 1998 to 2005 (Clayton, 2006). Table 1.1 and Table 1.2 list some of these academic and commercial platforms and describe their most important attributes.

Though significant technological achievements have been accomplished in the wireless sensor industry and various platforms are available on the market, some remaining constraints in their use for real damage detection applications are still present. Power limitations restrict their useful lifetime and performance. Time synchronization protocols are often needed to obtain useful data for SHM applications (Elson et al., 2002; Ganeriwal et al., 2003; Lynch et al., 2005; Maroti et al., 2004; Mechitov et al., 2004). Effective communication protocols are also needed for reliable data transmission (Mechitov et al., 2004). Therefore, middleware services are required to maximize the lifetime of these wireless sensors networks and ensure a reliable performance to examine the structural health condition after severe structural events. Spencer and Nagayama (Spencer and Nagayama, 2006; Nagayama et al., 2006; Nagayama, 2007) have also identified a more comprehensive set of research gaps in the development of SHM systems based on wireless sensors, including network scalability and adaptability,

network data loss, power efficiency, sensor environmental hardening, sensor resolution/range, and development of algorithms based on data fusion.

Consequently, data processing approaches that can exploit the on-board processing features offered by the wireless sensors to reduce large amount of communication and power consumption requirements are necessary. Such implementations are defined as distributed techniques. Under distributed techniques, on-board data aggregation tasks are implemented to define ideal data partitioning points leading to a considerable reduction of energy and power consumption for wireless transmission. Moreover, distributed implementations are versatile and typically scalable for large deployments with low power requirements. The next section highlights the importance of such distributed approaches in WSN applications and describes the distributed implementation pursued in this study.

1.1 The Importance of Distributed Techniques in SHM

Most existing damage detection techniques require a great deal of high-fidelity response data as well as significant computational power for real-world implementation. Centralized processing of global structural response data has been the standard. However, a new paradigm is needed to successfully employ wireless sensor networks in this application due to the severe resource and power constraints associated with these networks (Spencer and Nagayama, 2006). Properly implemented distributed processing algorithms will significantly reduce the power consumption and bandwidth requirements.

Battery-powered smart sensor platforms constitute a new possibility for developing damage detection systems based on distributed processing and wireless sensor networks (WSN). In addition to simply recording response data and transmitting it to a base station, more advanced wireless sensor platforms offer powerful on-board processing capabilities that are critical for performing the distributed computations. On-board

microprocessors are used to accomplish data aggregation and enable the sensors to only transmit a reduced set of processed information for additional analysis.

Robust damage detection techniques involving sophisticated and fault tolerant algorithms for damage detection are being studied (Sohn et al., 2004; Lynch, 2004). However, real implementations capable of functioning within the confines of a wireless sensor network continue to pose a significant research problem to the SHM community. Several WSN implementations have been performed to test their reliability under real sensing conditions. For instance, at Clarkson University researchers have implemented a wireless sensor system for modal identification of a full-scale bridge structure in New York (Gangone et al., 2007). Battery-powered wireless sensor nodes equipped with accelerometers and strain transducers are used having a high wireless data transmission rate. The entire network is polled by a master computer that collects acceleration and strain data. Both modal identification and quantification of static responses is performed using centralized network architecture. Figure 1.1 and Figure 1.2 show a view of the deployment and the wireless sensor setup used in this implementation, respectively. The wireless sensor platform is able to interact with an accelerometer and a strain transducer.



Figure 1.1 Wireless sensor nodes deployed on one of the beam girders (after Gangone et al, 2007)

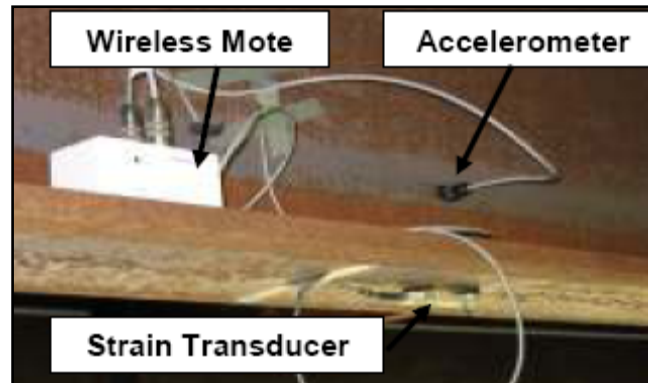


Figure 1.2 Wireless sensor setup (after Gangone et al, 2007)

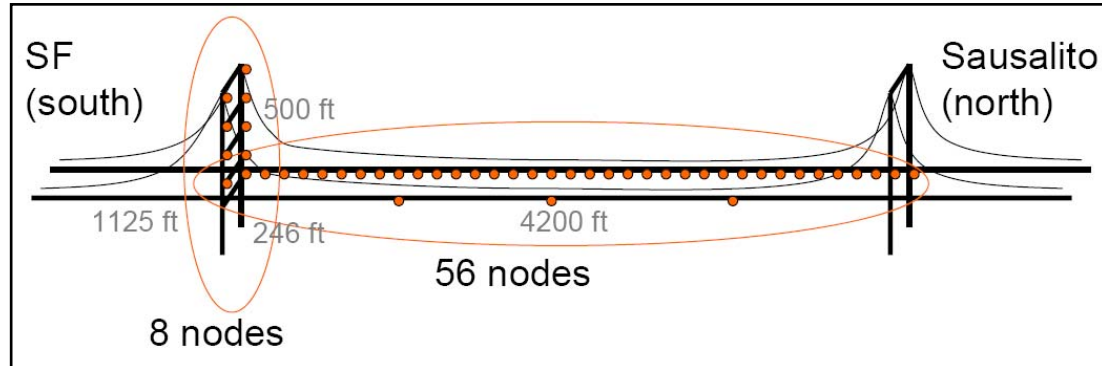


Figure 1.3 Layout of nodes deployed on The Golden Gate Bridge (after Kim et al., 2007)

In another real-world wireless sensor application, at the University of California, Berkeley (Kim, 2005; Kim, 2007; Kim et al., 2007; Pakzad et al., 2005) researchers have designed and deployed a wireless sensor network on the Golden Gate Bridge. The purpose of this implementation was to validate theoretical models and previous studies of the bridge. The deployment, considered the largest smart sensor network for structural health monitoring purposes, involves 64 nodes carefully distributed over the span and the tower measuring ambient vibrations synchronously at 1kHz in two directions. The data, reliably transmitted by using a 46 hop network with a bandwidth of 441B/s at the 46th hop, is collected using a base station (i.e., centralized network architecture) where frequency domain analysis is used to extract modal parameters. The total time required to transmit response data from all nodes to the base station is 9 hours, resulting in a system lifetime of 10 weeks when four 6V batteries are used as a power source.



Figure 1.4 Panoramic view of road test deployments (after Pei et al., 2008).

Figure 1.3 shows the nodes layout used in the Golden Gate Bridge implementation. As observed, 56 nodes are located along the bridge deck and the rest 8 along the left tower; all of them broadcasting data in a centralized architecture.

Other smart sensor applications in infrastructure systems have been reported. At the University of Oklahoma researchers have conducted and presented preliminary results for an experimental investigation to detect road weather conditions using a smart sensor network (Pei et al., 2008; Ferzli et al, 2006). In the implementation, a network of Mica2 motes, interfacing with three environmental sensors, are deployed to monitor pavement temperature and moisture to detect icy road condition. Sensed data, transmitted across the network and collected at a base station, is subsequently processed to categorize pavement surface conditions. In the study, several experiments were also performed to test communication interference due to traffic using a small-scale sensor network in a pseudo-field environment. Figure 1.4 shows a panoramic view of two road test deployments. The deployments include a network of five motes. The motes collect data and send it back to base station (Node 0) in a centralized architecture.

Clearly, with potentially hundreds of nodes sensing and streaming data at high sampling rates, the energy consumption and power requirements of these centralized approaches do not match the capabilities offered by wireless sensors, and therefore are not scalable for realistic damage detection applications. The development of distributed approaches that minimize data transmission, and thus power consumption, is necessary. On-board

processing capabilities using wireless sensors are successfully being exploited to perform data aggregation, thus reducing the wireless communication load (Lynch et al., 2004; Chintalapudi et al., 2006; Nagayama, 2007; Hackmann et al., 2008).

A distributed approach, amenable for local processing on the motes, has been proposed by Chintalapudi, et al. (2006). In this study, two qualitatively different SHM applications for damage detection and localization are tested using a small and medium-scale structures and NetSHM prototype. The damage detection was accomplished by analyzing shifts in modal frequencies, while damage localization based on mode shape changes. However, due to memory and processing capacity constraints in the platform (MicaZ), the technique evaluation was performed without involving any local processing on the smart sensors.

Additionally, Lynch et al. implemented a wireless sensing unit configured with an autonomous execution of an embedded damage detection algorithm (2004). The algorithm, based on statistical pattern recognition damage detection using AR and ARX time-series models, was tested using an eight DOF laboratory test structure. A fifty percent reduction in energy was reported by performing the damage detection at the sensor node as compared to using a centralized approach.

Researchers at the University of Illinois at Urbana-Champaign have experimentally validated a SHM system employing a smart sensor network deployed on a scale three-dimensional truss model (Spencer and Nagayama, 2006; Nagayama, 2007). Their approach includes implementation of the Distributed Computing Strategy (Gao, 2005) in which data is processed on iMote2 smart sensor communities under a hierarchical architecture. The algorithm includes the use of the eigensystem realization algorithm (ERA) (Juang and Pappa, 1985) and the damage locating vector method (Bernal, 2002) to exploit the on-board processing capacity of the iMote2.

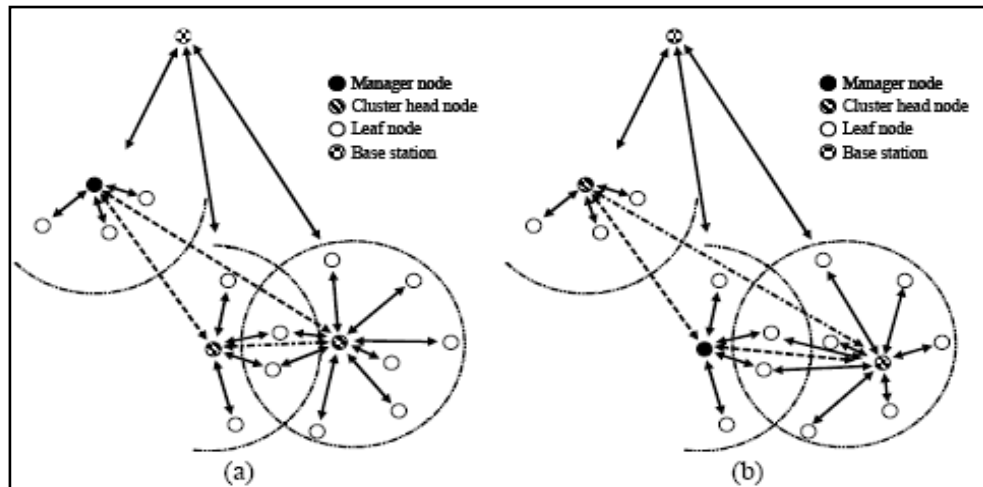


Figure 1.5 Examples of SHM implementations under hierarchical architectures (after Spencer and Nagayama, 2006)

Results demonstrated that the adopted SHM system is effective for damage detection and localization, and is scalable to a large number of smart sensors. Figure 1.5 shows two examples of SHM implementations under a hierarchical architecture. “Leaf” nodes collect data and process it in parallel to the “cluster head” nodes. Final results are collected by the “manager” node and sent to a base station.

These previous approaches do require a considerable amount of communication between sensor nodes which will draw a significant amount of energy. In this thesis, a distributed damage detection approach involving low power requirements is proposed and validated. The wireless sensor network is implemented to experimentally validate the distributed damage detection system. The study proposes an analysis that can be viewed as taking place in two stages. The first stage exploits the on-board microprocessor resources of the wireless sensors to perform frequency identification using the measured acceleration data. As a result, only a very limited number of intermediate parameters are transmitted wirelessly to the base station. The second stage computes and examines correlation factors to detect and localize damage. The in situ experimental validation of this damage detection system is conducted using two experimental structures of increasing

complexity. The first structure to be considered is a simple cantilevered beam. The second deployment focuses on a more complex truss structure.

1.2 Overview

This study is focused in the development and experimental validation of a completely distributed damage detection system that has minimal power requirements and will be effective for identification of potential damage zones in a structure. The damage detection system is implemented on a wireless sensor network and in situ validation is performed. With the proposed approach, the communication load and power requirements are considerably reduced by exploiting the local processing capabilities offered by the wireless sensors. Nearly all required computation is performed on-board the sensor platforms, and a reduced amount of data is transmitted to a base station for a final computation and decision phase.

Chapter 2 focuses on the background and implementation of the proposed approach. The four implementation steps are introduced and an optimal partitioning point in the data aggregation flow is highlighted. Data acquisition, data processing, data transmission and damage localization steps are discussed in detail. The specific sensor board selected for the data acquisition is presented and its main features and limitations observed during the experimentation are discussed. On-board data aggregation, including the frequency domain transformations and curve fitting technique, is described. The wireless sensor platform selected for this validation, the *iMote2*, is described and its main characteristics and capabilities are discussed. The communication protocol used to achieve a reliable data transmission is also described. Statistical evaluation of latency and energy usage is summarized to demonstrate that minimal energy is required using with the proposed implementation of this distributed approach. The Damage Location Assurance Criteria (DLAC) method, developed by Messina, et al. (1996) and first proposed for wireless sensor networks by Clayton et al. (2005) is studied. Limitations and restrictions involved in this methodology are evaluated. A user interface to allow the user to interact with the network for experimental validation steps is presented and described.

Chapter 3 and Chapter 4 focus on the experimental validation of the proposed distributed damage detection system. The system is deployed and validated on two experimental structures of increasing complexity using a wireless sensor network (WSN). With very little energy usage the system is experimentally demonstrated to be capable of detecting the damage zone for both cantilevered beam and 3D truss structures. The experimental setup for each experiment is explained. Damage detection patterns, required by the correlation-based damage detection technique proposed in this study, are developed based on a finite element model. Therefore the mathematical idealizations of the numerical models used to accomplish the required damage patterns are discussed. Experimental results are then presented and discussed. Additional off-line analyses using the experimental results and numerical studies are presented to test the reliability of the proposed distributed algorithm under other damage locations and other realistic damage patterns.

Chapter 5 finalizes the dissertation, presenting conclusions and proposing further research steps in damage detection implementations with distributed strategies.

Chapter 2

Distributed Damage Detection System Implementation

In this chapter the damage detection system is described. The damage detection system is completely distributed and is implemented using wireless sensor platforms configured with a single hop network from a base station. All network sensors operate independently of each other and no communication is required between them. The system is based on correlations of the frequency changes of an experimental structure and an analytical model, and the analysis is performed in two stages. The first stage uses raw acceleration data acquisition to perform frequency identification at the sensor platform using the onboard processing abilities. Processed data are then wirelessly transmitted to the base station where the second stage is performed to compute correlations and localize damage.

2.1 Overview

The entire implementation is configured in four steps and parameterized by N , the number of acceleration samples at each sensor platform, and W , the number of natural frequencies to be identified. A general flow chart of the entire implementation is provided in Figure 2.1.

The first of the four steps is **Data Acquisition**, where a set of N integer acceleration readings are acquired for use in the next step.

The second implementation step, **Data Processing**, is then performed using three routines run consecutively. First, a Fast Fourier Transform (FFT) routine is initially applied to translate the N integer readings into N floating-point values to obtain the frequency domain representation of the raw data.

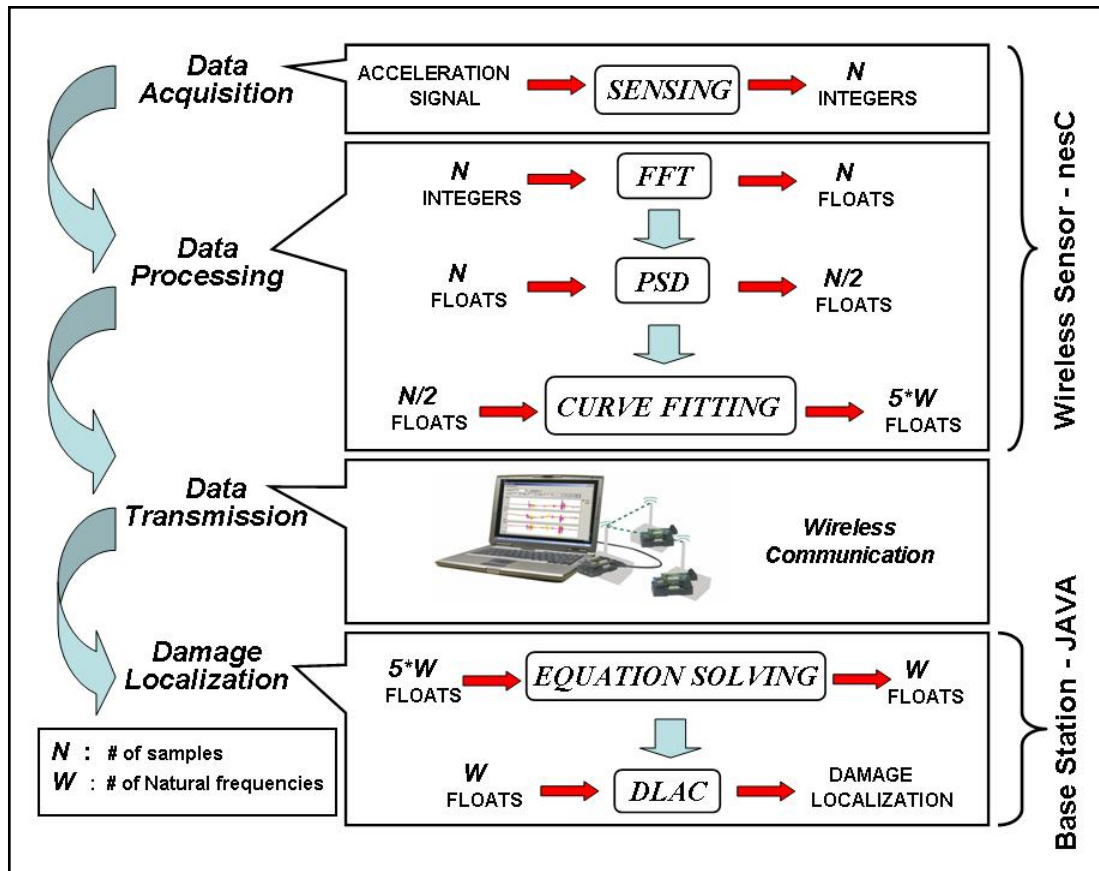


Figure 2.1 Flow chart of implementation

Then, a second routine is run to transform the N floating-point values into $N/2$ floating-point values by calculating the Power Spectral Density (PSD) function using the FFT data. Finally, a curve fitting routine is used to perform a parameters extraction task to reduce the PSD data to $5*W$ floating-point values.

Next, **Data Transmission** is performed to wirelessly transmit the curve fit parameters from each sensor platform to the base station.

Finally, **Damage Localization** is performed using two additional routines and the curve fit parameters received from the sensors. An equation solver is used to reduce the previous curve fit parameters to a set of W floating-point values, i.e. the natural frequencies of the structure. Finally, correlation values, based on experimental and

analytical frequency change vectors, are calculated to localize potential damage in the structure.

As observed, a significant communication load reduction offered by the distributed strategy is achieved by the appropriate selection of data partitioning. An appropriate partitioning point in the data aggregation flow is set just before the data transmission step, therefore a minimal power is required for wireless transmission because the amount of information is reduced by several orders of magnitude ($N \gg 5*W$).

Each of the proposed implementation steps are described in the following sections. A user interface, based on a Java program, is also developed to set experiment parameters and govern which tasks are to be conducted within the experiment. The interface is also described at the end of this chapter.

2.2 Data Acquisition

Acceleration data acquisition is performed as a first step through the proposed damage detection system. Raw acceleration data is measured using the on-board sensor, which is described in the next section. The data is then fed into the data processing step to identify the natural frequencies of the system by performing frequency domain transformation and curve fitting tasks.

2.2.1 Sensor Board

A basic sensor board (ITS400), developed by Intel Research Lab and designed to interact with the *iMote2* platform selected for this implementation (discussed in detail in section 2.3.4), is used to perform the acceleration acquisition. The basic sensor board has embedded a digital accelerometer (ST Micro LISL02DQ) with additional sensors to measure temperature, humidity and light. Four A/D converters are available on the sensor board platform. The A/D converter allows for an analog-to-digital conversion of the data. The quantification of the analog signal to a discretized value is performed based on a given resolution in number of bits. Once the signal is acquired, each of its values is

rounded to a discrete level defined by the number of bits. For instance if $r = \#$ of bits, then, $2^r - 1$ discrete levels are produced.

The digital accelerometer on the sensor board offers 12-bit resolution, or equivalently 0.97 mg of resolution based on the $\pm 2g$ range and configured for 3-axes of measurement with a limit of 3000 data points per axis. However, only 2048 points are used in this study ($N=2048$). A photo of the basic sensor board is shown in Figure 2.2.

In accordance with Nyquist sampling theory, sampling must occur at a frequency of at least twice the largest significant frequency component present in the signal. If this condition is not fulfilled, a phenomenon called *aliasing* occurs. The aliasing causes frequency components with a larger value than the Nyquist frequency to be aliased to lower frequencies. The Nyquist frequency value is shown as

$$f_N = \frac{1}{(2T)} \quad (2.1)$$

where

f_N : Nyquist frequency

T : Sampling period

Therefore, a sampling frequency greater than twice the highest frequency component in the signal must be selected to avoid aliasing. However, in real applications it is impossible to obtain a band-limited signal, and aliasing always will be present at some level. To reduce this complication, an analog low-pass filter must be applied to the signal prior to sampling to attenuate the frequency components greater than a selected cutoff frequency. The cutoff frequency must at least be lower than the Nyquist frequency to reduce aliasing.

The digital accelerometer on the sensor board allows for A/D conversion at the sensor i.e., on-board. Therefore a digital output is available after the sampling is performed.

Sampling frequencies and corresponding cutoff frequencies must be previously set on the *iMote2* using digital filters and the user-defined decimation factors given in Table 2.1. Specifications available for the accelerometer explain that once the decimation factor is defined, the sampling frequency and resultant cutoff frequency will have a value within +/-10% of the value set by the user. For instance, if a decimation factor were defined as 64, the sensor would operate with an actual sampling frequency between 504-616 Hz (i.e., not precisely at 560 Hz). Consequently, sampling frequency values will actually vary from sensor to sensor.

The actual values may be determined using an oscilloscope prior to experimentation or by a self-calibration routine embedded in the sensor platforms. However, on a given sensor a consistent sensing frequency was observed (i.e., there is no variation in the sampling frequency value with time).

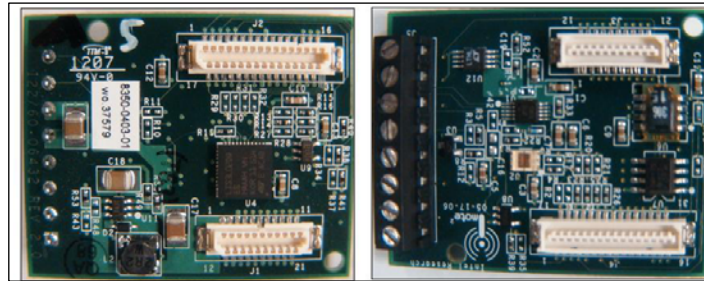


Figure 2.2 Top and bottom view of basic sensor board

Table 2.1 Accelerometer user specified sampling rates

Decimation Factor	Cutoff Frequency (Hz)	Sampling Rate (Hz)
128	70	280
64	140	560
32	280	1120
8	1120	4480

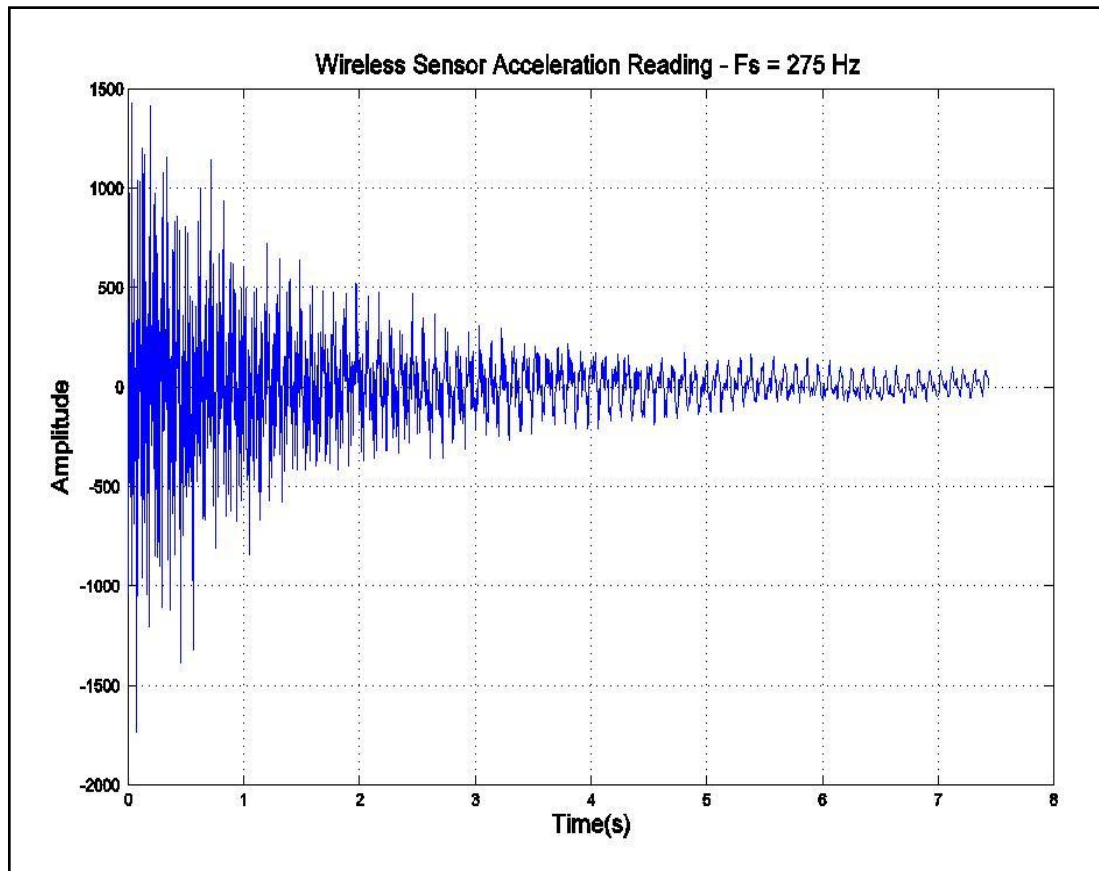


Figure 2.3 Wireless sensor time history record

For illustration, a typical acceleration record of 2048 samples is shown in Figure 2.3. The data, lasting approximately 7.5 sec, corresponds to a cantilevered beam structure under impulsive lateral vibration. A sampling frequency of 280 Hz and cutoff frequency of 70 Hz are selected. However, as explained before, the data is acquired with an actual operating sampling frequency of 275 Hz corresponding to the 98.20% of the expected value.

2.3 Data Processing

As previously mentioned, three consecutive routines are applied in this step to perform frequency identification of the structure at the sensor level. The raw acceleration data is stored in the local memory on the *iMote2*. A program running on each of the motes (implemented in the *nesC* programming language) is designed to process the

acceleration data and perform modal identification. The Fast Fourier Transform (FFT), Power Spectral Density (PSD) and a curve fitting technique are discussed in the following sections.

2.3.1 Fast Fourier Transform (FFT)

The Discrete Fourier Transform (DFT) is required, as the first task in the data processing step, to perform a time-frequency domain transformation of the acceleration data. The DFT is calculated as

$$X_k = \sum_{n=0}^{N-1} x_n W_N^{kn} \quad (2.2)$$

$$W_N = e^{\frac{-j2\pi}{N}} \quad (2.3)$$

where

X_k : “ k -th” complex DFT value

x_n : “ n -th” time domain sample

N : Number of samples

However, a direct DFT computation is not efficient to embed on the microprocessor. To compute the N values of the DFT would demand $N^2 - N$ complex additions and N^2 complex multiplications. Therefore, a more computational efficient algorithm is required.

The Fast Fourier Transform (FFT) based on the Cooley and Tukey algorithm, (Cooley and Tukey, 1965) computes the same result much faster. The FFT algorithm is able to compute the DFT of N values in only $O(N \log_2 N)$ operations. When a long data set is transformed, this computation speed advantage is more evident. Thus, once the acceleration data are acquired, an N -point FFT routine, implemented on the wireless

sensor microprocessor, is applied to transform the discrete-acceleration time signal in the frequency domain. The output is then fed into the next step to calculate the power spectral density function as explained in the next section.

2.3.2 Power Spectral Density (PSD)

Power spectral density values P_k are calculated as the squared magnitude of the prior complex FFT values using the equation

$$P_k = \frac{X_k X_k^*}{N} \quad (2.4)$$

where

X_k : “*k-th*” complex FFT value

X_k^* : “*k-th*” complex conjugate FFT value

N : Number of samples

If the unmeasured disturbances to the structural system are white noises (ie., have flat PSDs), the PSD of the response may be viewed as a system transfer function. However, even in the case when the input is not white, this approximation has been found to be appropriate for determination of the frequencies of the system. Recall that the objective is only to identify the frequency locations. Therefore, the PSD of a response record in which all of the modes are excited up to a desired bandwidth level may still be used. For instance, the response of impact testing will produce a corresponding PSD with different amplitude as the system transfer function. However the peaks in the PSD will clearly be identical to those in the transfer function.

The structural frequency values may then be accurately determined using the curve fitting technique discussed in the following section. Data obtained with each sensor are processed entirely at that particular sensor node and no transmission of the raw acceleration data is needed to implement the algorithm.

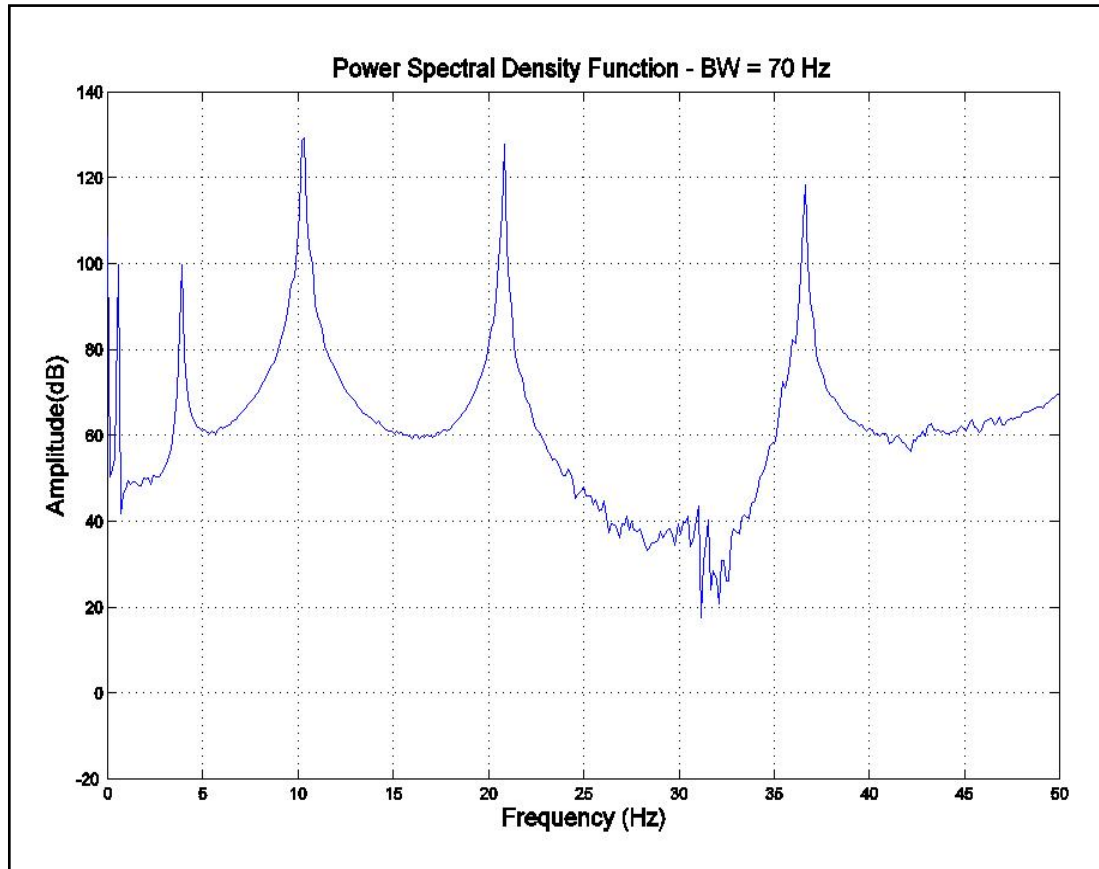


Figure 2.4 Corresponding Power Spectral Density Function.

Figure 2.4 shows a typical PSD plot where five resonant frequency locations, corresponding to the peaks, can be distinguished. The PSD record corresponds to the time domain acceleration record shown in Figure 2.3.

2.3.3 Curve Fitting Technique

A curve fitting technique found to be successful in previous applications for lightly damped systems is applied to the PSD function to determine the natural frequencies. A fit of the PSD data immediately surrounding each of the modes is performed to identify each frequency. Levi's approach is used to accomplish the curve fitting (Levy, 1959). This approach was proposed in prior related studies (Clayton et al., 2005; Clayton et al., 2006; Clayton, 2006) and enables one to identify the natural frequencies by determining the parameters that result in a least-squares fit of a fractional polynomial expression to

the frequency domain data. The fractional polynomial is defined as a ratio of two complex polynomials in terms of unknown coefficients a_i , b_i , as in

$$G(i\omega) = \frac{a_0 + a_1(i\omega) + a_2(i\omega)^2}{b_0 + b_1(i\omega) + b_2(i\omega)^2} \quad (2.5)$$

The values of the fractional polynomial coefficients in equation 2.5 are obtained by minimizing the weighted sum of the squares of the errors between the magnitude of the proposed $G(i\omega)$ and the experimental frequency domain data. Once the error function is minimized, a linear equation system whose variables are the unknown coefficients of $G(i\omega)$ is produced. The procedure is now summarized. If $H(i\omega)$ represents the experimental frequency domain data, then the numerical difference (error) between the two functions, i.e. $H(i\omega)$ and $G(i\omega)$ is defined as

$$\varepsilon(\omega_k) = H(i\omega_k) - G(i\omega_k) = r(\omega_k) + is(\omega_k) \quad (2.6)$$

where

$\varepsilon(\omega_k)$: Numerical difference at any particular frequency ω_k

$r(\omega_k)$: Real component of the numerical difference at any particular frequency ω_k

$s(\omega_k)$: Imaginary part of the numerical difference at any particular frequency ω_k

Then, a function describing the weighted sum of the squares of the errors is defined as

$$E = \sum_{k=0}^{fs/2} [r^2(\omega_k) + s^2(\omega_k)] = f(a_0, a_1, a_2, b_0, b_1, b_2) \quad (2.7)$$

Finally, the error function E is minimized with respect to the coefficients a_i , b_i to obtain the parameters of a linear equation system, as previously mentioned. This technique can also be modified for PSD curve fitting calculations by considering the complex part of the $H(i\omega)$ to have a zero value. The parameters (coefficients of the

linear equation system) calculated with the PSD are then transmitted wirelessly to the base station as input for the fourth implementation step.

Once the coefficients of $G(i\omega)$ are determined, the natural frequencies are obtained as the roots of the polynomial denominator, i.e. the imaginary part of the poles of the system. Figure 2.5 illustrates the results of fitting a second order fractional polynomial at each of the five peaks ($W=5$, number of frequencies to be captured) of the previous PSD shown in Figure 2.4. In this example, the PSD is used as the experimental frequency domain data.

Because we are fitting the data in the region surrounding each peak, the denominator has a known polynomial order of two, i.e., the number of poles is equal to two times the number of frequencies to be captured. The curve fit procedure is repeated for each of the frequencies to be identified. Therefore, appropriate frequency intervals to perform the curve fitting routine for each peak are previously selected and defined using the user interface developed for this application (see Figure 2.8). Each interval is expected to contain each of the peaks. For instance, the fourth peak on the PSD record is contained in an interval ranging from 18Hz to 28Hz. These values are inserted in the user interface as observed in Figure 2.8. The same process is then repeated for each of the five peaks selecting other frequency intervals. The selected frequency intervals are not restricted by specific limits or values. However, it is expected to have better curve fitting results if the selected frequency interval contains more frequency points to include in the error function E .

Remember that the objective pursued in this analysis step is the identification of the natural frequencies of the structure, as roots or poles of the denominator in the fractional polynomial, i.e., a transfer function mathematically obtained. Therefore, the amplitudes of the fitted curves are irrelevant and unnecessary for this calculation. Figure 2.5 shows that the amplitudes of fitted curves may not be the same as the PSD data but the frequency locations are correctly identified

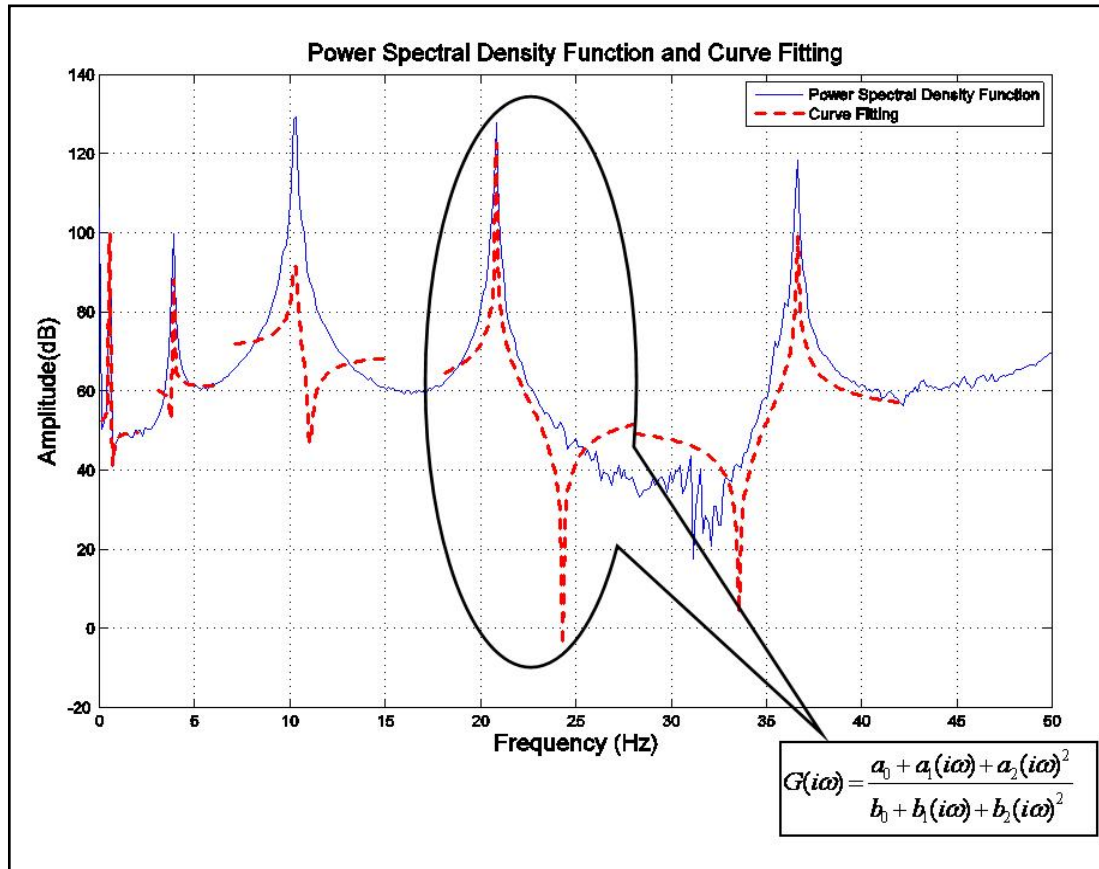


Figure 2.5 Sample Power Spectral Density and Curve Fit

2.3.4 *Imote2* Platform

The *iMote2* (IPR2400) is selected as an advanced wireless sensor platform which offers adequate processing power to accomplish the FFT, PSD and curve fitting routines described on the previous sections. Its main board has a low power 416MHz PXA271 XScale processor with 256 KB of integrated SRAM and 32 MB of external SDRAM, embedded in a modular compact size of 48 x 36 x 7 mm with analog and digital interface connectors to interact with sensor and battery boards. Data transmission is accomplished by the use of an 802.15.4-compliant 2.4 GHz radio (Chipcon CC2420) integrated with a built-in antenna. Power can be provided by a battery board or via the integrated USB interface.

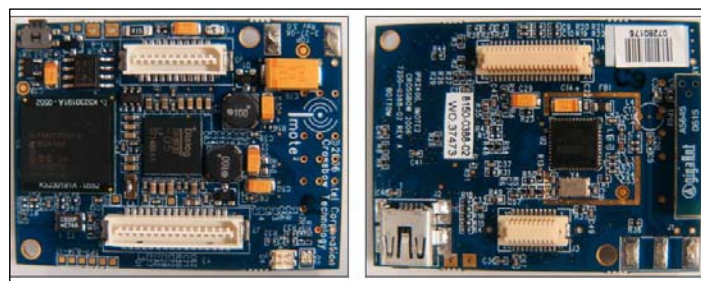


Figure 2.6 Top and bottom view of *iMote2* main board

Table 2.2 *iMote2* Main Board Properties

Microprocessor	XscalePXA271
Active Power (mW)	44 @ 13 MHz, 570 @ 416 MHz
Clock speed (MHz)	13 - 416
RAM (bytes)	256 K + 32 M external
Program flash (bytes)	32 M
802.15.4 radio (ChipCon 2420)	

Other important *iMote2* main board features can be observed in Table 2.2. This choice of smart sensor platform made it possible to implement this completely distributed approach for structural damage detection. A photo of the unit is shown in Figure 2.6.

2.4 Data Transmission

As previously explained, the set of $5*W$ coefficients associated with the model fitted to the PSD are calculated on the smart sensor platform and transmitted to the base station. These values are transmitted from the *iMote2* to a PC base station wirelessly through a gateway mote. The gateway mote, receives the data packets from the sensors using an 802.15.4-compliant 2.4 GHz radio (Chipcon CC2420) integrated with a built-in antenna, and relays the data to the PC over a USB cable. The PC base station completes the damage localization implementation step and provides the results (DLAC coefficients) to the user with a Java interface.

Although the purpose of this study is to validate a distributed implementation, the application is written to be flexible and to facilitate debugging and validation. Thus, raw acceleration data is also available for transmission to the base station for debugging and

validation purposes. Therefore, a reliable transport layer is implemented to achieve reliable data transmission from the wireless sensor platforms to the base station. The reliable transport layer is tailored for the specific features of the *TinyOS 1.1.15*. Operating System (TinyOS, <http://www.tinyos.net/>). The transport layer divides sensor data into packets small enough for the radio protocol stack to handle, transmits all the data packets to the base station, and reassembles them upon arrival. Additionally, an Automatic Repeat Request procedure (ARQ) is implemented to detect and retransmit lost packets during communication. After a sender sends a data packet to the base station, it waits for an acknowledgment from the receiver. If an acknowledgment is not received within 0.5sec it will retransmit the data packet. This process is repeated until an acknowledgment is received, at which time the sender mote proceeds to the next data packet. To detect duplicate data packets, each data packet has a sequence number differentiating it from the other packets. Therefore, the base station accurately reassembles the original block of data after all of the packets are received. Each packet consists of 15-bytes of data, and a sequence number for a final re-assemble process. For this study, sender *iMote2* motes are configured to send a 12,352 byte block data to the base station divided into 12,288 bytes for payload and 64 bytes for the header.

This communication protocol was verified experimentally using seven wireless sensors, located 16 feet from the base station. Obstacles such as metal bookcases were placed between the base station and the wireless sensor deployment to observe performance. To detect communication failures, a pattern of bytes was written into the block data before sending it to the base station which is configured to verify if the pattern of bytes still exists after transmission is concluded. The pattern of bytes used was a counter that repeatedly goes from 0x00 to 0xFF. Through the test, each of the seven *iMote2* wireless sensor sent their block data to the base station sequentially. All of the data from the network arrived successfully, which confirmed the communication protocol is reliable.

In the next section, a summary of a statistical evaluation in terms of latency and energy consumption is provided to appreciate the advantages of the proposed distributed implementation (Hackmann et al., 2008).

2.4.1 Latency and Data Reduction Analysis

An evaluation of latency and data reduction is introduced in this section to highlight the advantages of the present distributed approach. The evaluation is performed by analyzing the execution time for the computational tasks performed on-board and the wireless transmission from the sensor to the base station (Hackmann et al., 2008). The corresponding times are measured using the *iMote2* onboard microsecond timer. Additionally, the time incurred to transmit the data from the sensor to a base station under a centralized approach is also measured for comparison purposes. Table 2.3 shows the measured execution times for the proposed distributed approach and an opposite centralized approach in which all the raw data is transmitted to the base station.

The analysis is performed using $N=2048$ samples and $W=5$ natural frequencies. The same parameter values were used in prior illustrative examples and are used later for the actual experimental validation. As observed in Table 2.3, both approaches require the same time (3772 ms) to collect all the raw data. The distributed approach requires 681.1 ms to accomplish the remaining computational tasks on-board, while the centralized approach does not perform any computational on-board tasks. Finally, the distributed approach requires 270 ms to send the curve fitting parameters to the base station, while the centralized procedure requires 9638 ms to transmit the entire set of raw data to the base station. Consequently, the proposed distributed approach is able to achieve latencies **64.8 %** lower than those of a centralized approach.

Table 2.3 Latency Analysis Table

	<i>Distributed</i>	<i>Centralized</i>
	<i>Time (ms)</i>	<i>Time (ms)</i>
Raw Data Collection	3772	3772
FFT	566.8	0
PSD	17.1	0
Curve Fitting	97.2	0
Wireless Transmission	270	9638

Moreover, under a centralized approach without exploiting the on-board processing capacity offered by the sensor platforms, 2048 integer sensor readings would have to be transmitted back to the base station. However, under the distributed approach only partial results consisting of $5*W = 25$ floating-point curve fitting parameters are transmitted back to the base station for final calculation. Therefore, a **98.8%** of data reduction is also accomplished with the proposed approach.

2.4.2 Energy Usage Analysis

Additionally, energy consumption is evaluated using the previous latency analysis results in conjunction with the current consumption information for radio, sensor and CPU provided by the manufacturers (STMicroelectronics, 2005; Crossbow Technologies, 2007). Again, the evaluation is performed by analyzing the energy consumption for the computational tasks performed on-board and the wireless transmission from the sensor to the base station (Hackmann et al., 2008). The results indicate that the presented distributed processing approach reduced the energy usage to 0.067 mAh in contrast to 0.222 mAh that a centralized approach would require. Therefore, the proposed distributed approach is able to achieve an energy reduction of almost **70.0 %** lower than that of a centralized approach. This reduction is due mostly to the fact that no raw data is sent to the base station. The distributed approach only incurred in 0.006 mAh for the on-board computation instead of 0.160 mAh that it would be needed to transmit the entire raw data set to a base station under a centralized approach.

2.5 Damage Localization Algorithm

Once the set of partial parameters from the curve fitting routine are transmitted to the base station, a java code placed at the base station is used to perform the fourth implementation step by obtaining the natural frequencies and correlation coefficients to detect and localize damage. The natural frequency values are calculated with an equation solving routine. Then, the Damage Location Assurance Criterion (DLAC) technique is used to compute the correlation values.

The main features and mathematical considerations involved in each of the routines performed at this implementation step are explained in the following sections.

2.5.1 Equation Solver

The equation solver involves three consecutive tasks. First, a linear equation system is defined in terms of the curve fitting parameters. Then, the linear equation system is solved to determine the unknown coefficients of the fractional polynomial $G(i\omega)$ defined in equation 2.5. Finally, the roots of the fractional polynomial expression are calculated. The resulting roots, the poles of the system, contain the required frequency information. The expression for the fractional polynomial denominator is defined as

$$b_0 + b_1(i\omega) + b_2(i\omega)^2 = 0 \quad (2.8)$$

the roots are then calculated using the quadratic equation

$$i\omega = \frac{-b_1 \pm \sqrt{b_1^2 - 4b_2b_0}}{2b_2} \quad (2.9)$$

where each solution takes the form

$$i\omega = \zeta\omega_n + \omega_d i \quad (2.10)$$

and

ω_n : Undamped natural frequency in radians

ω_d : Damped natural frequency in radians

ζ : Damping ratio

Because we are only interested in the imaginary part, then the natural frequency values are calculated as

$$f = \frac{\omega_d}{2\pi} \quad (2.11)$$

where

f : Damped natural frequency in Hertz

Thus, the equation solver routine reduces the previous set of $5*W$ floating-point curve fitting parameters to a set of W floating-point values i.e. the natural frequencies of the system. These values are then fed into the next routine to compute correlation values and detect damage.

2.5.2 Damage Location Assurance Criterion (DLAC)

Typically, SHM techniques detect, localize and quantify structural damage by analyzing modal information identified from the structure. Correlation-based damage detection techniques identify damage by comparing changes in modal parameters obtained by experimental and numerical approaches. Messina proposed the Damage Location Assurance Criterion (DLAC) (Messina et al., 1996; Messina et al., 1998) as an adaptation of the Modal Assurance Criterion (MAC) (Contursi et al., 1998) technique for damage detection. MAC measurements are usually used to validate the accuracy of analytical models produced by experimental tests while DLAC approach identify damage by evaluating the linear correlation between frequency change vectors obtained by experimental measurements and an analytical model. The experimental natural frequencies are calculated as the imaginary part of the poles of each fractional polynomial as explained in the curve fitting section (Section 2.3.3). The DLAC value is calculated as

$$DLAC_j = \frac{|\{\Delta\omega\}^T \{\delta\omega_j\}|^2}{(\{\Delta\omega\}^T \{\Delta\omega\})(\{\delta\omega_j\}^T \{\delta\omega_j\})} \quad (2.12)$$

where

$$\Delta\omega = (\omega_{healthy} - \omega_{damage}) / \omega_{healthy} \quad (2.13)$$

$$\delta\omega_j = (\omega_{healthy}^a - \omega_j^a) / \omega_{healthy}^a \quad (2.14)$$

ω : Vector of natural frequencies obtained with experimental measurements

ω^a : Vector of natural frequencies obtained with the analytical model

Equation 2.12 represents the linear correlation between frequency change vectors. Frequency change vectors for experimental and numerical models are denoted by $\Delta\omega$ and $\delta\omega_j$, respectively. These vectors are normalized with respect to the corresponding healthy natural frequencies using equation 2.13 and equation 2.14 to equally weight all vectors and reduce any bias induced by higher modes. Note that the outcome of this equation is restricted to positive values between 0 and 1. A concentration of relatively high DLAC values indicates strong correlation and therefore a potential damage location.

Note that this approach requires the selection of an assumed damage detection pattern to produce frequency change vectors for the numerical model. The j th damage detection pattern describes the numerical values of the natural frequencies for a particular damage level and site. Damage is inherently nonlinear, but because the structure is experiencing ambient vibration before and after damage occurs, linear models are used to represent the structure in both cases. Although the DLAC values are dependent on both the level and location of the assumed damage, the DLAC's ability to detect damage is robust, because frequency change vectors are normalized and their magnitude is unnecessary for the calculation. However, some uncertainties present during an actual implementation of the DLAC have been found to affect its reliability (Clayton, 2006). Clayton performed an assessment of the DLAC accuracy in previous numerical studies using a cantilever

beam model. In his study it was concluded that the reliability of the DLAC to detect damage is dependent on having a sufficiently refined analytical model. The success of the method is also dependent on the noise distribution present in the output signals. These effects are later evaluated in a numerical simulation using an analytical model of a truss.

Because the DLAC approach is only applicable to detect individual damage events, extensions of this technique may be considered to detect multiple damage locations (Koh and Dyke, 2007) or to detect damage in perfectly symmetric structures. However these would not allow for a completely decentralized approach. Also, a sufficient number of modes must be employed. If the number of modes is not sufficient, the frequency change vector can result in strong correlation with more than one damage patterns, limiting the usefulness of this approach for real structural damage localization.

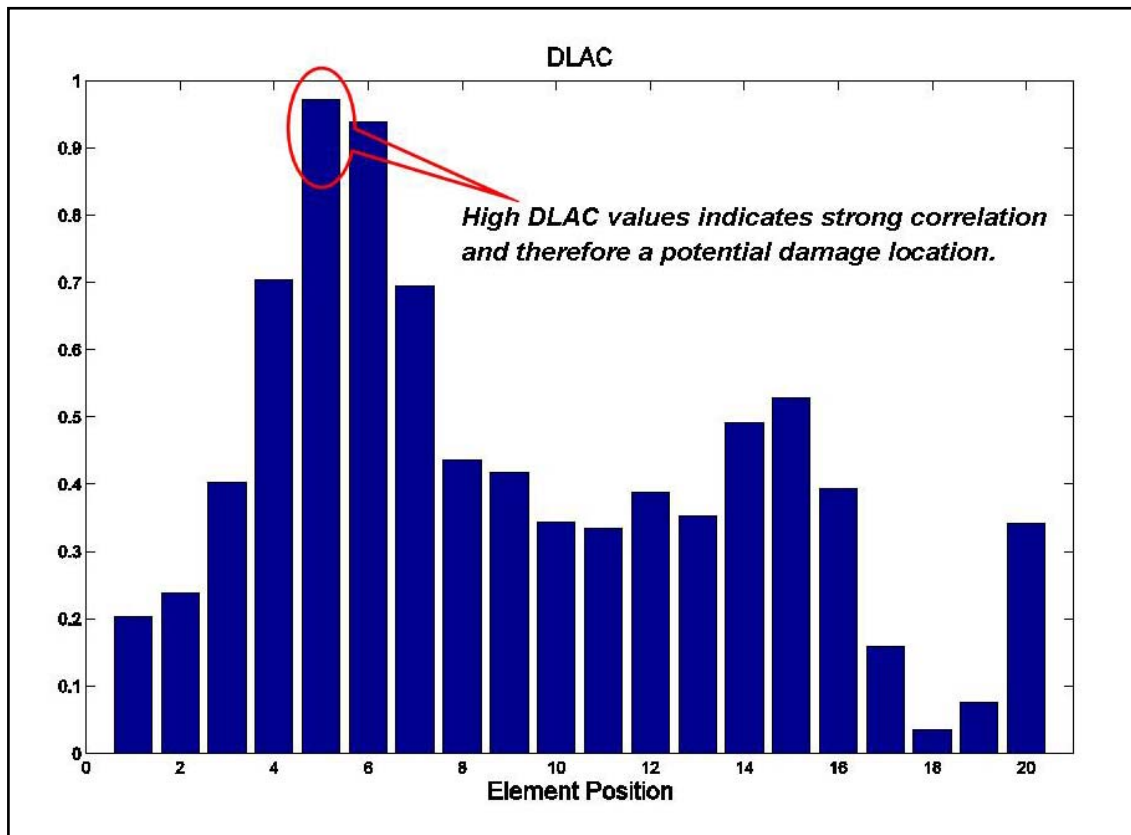


Figure 2.7 Correlation Factors calculated with the DLAC

Figure 2.7 shows a typical DLAC output related to the previous cantilevered beam data shown in Figure 2.3. The correlation factors, associated to a damage detection pattern of twenty possible damage locations, show a potential source of damage between the fifth and sixth locations.

2.6 Description of User Interface

A Java application was also developed as a user-interface to monitor and control the entire network and define the sensing parameters. Figure 2.8 shows the user-interface developed for this implementation.

The proposed interface enable users to set sampling frequencies for sensor boards, initialize the application and save results for post-processing. Because the curve fitting is applied at each peak in the PSD record then a selection option of curve fitting intervals in the frequency domain is also available. Additionally, raw and corresponding power spectrum data may be requested and recorded for debugging purposes.

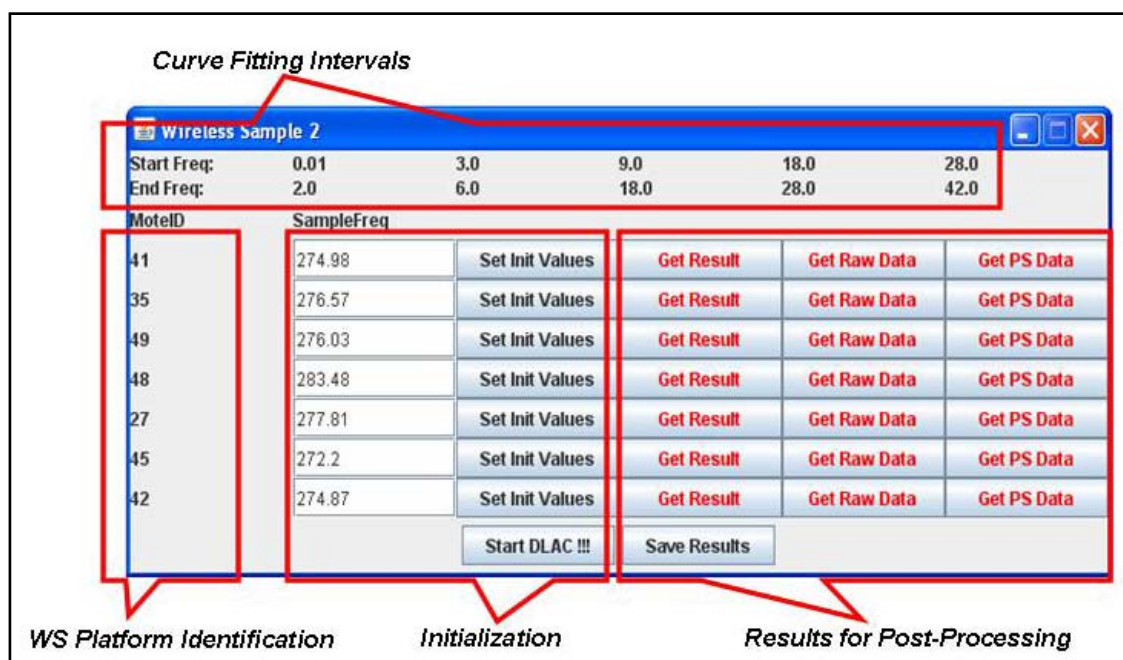


Figure 2.8 User-interface

2.7 Summary

The need for SHM schemes to exploit on-board processing capacity of wireless sensors to perform data processing tasks in-situ is highlighted in this chapter. A distributed damage detection system based on the use of a wireless sensor network is proposed. A detailed description of the entire implementation is provided. Four analysis steps are explained and their roles in the damage detection system are discussed. An optimal partitioning point in the data aggregation flow is presented leading to a considerable reduction of communication load, latency and energy usage in the system. This approach enables scalability of the system using a dense wireless sensor network. The Damage Location Assurance Criteria (DLAC) is presented as a suitable damage detection technique to be utilized in the proposed distributed scheme.

Chapter 3

Cantilevered Beam Experiment

In this chapter an initial experimental validation of the proposed distributed damage detection approach is performed using a wireless sensor network deployed on a simple experimental structure. A steel cantilevered beam, located in the Structural Control and Earthquake Engineering Lab at Washington University in St. Louis (Clayton et al. 2005; Clayton 2006) is selected as the experimental specimen. The structure is excited in the lateral direction yielding bending vibration. This initial experiment also provides opportunities to realize some of the basic constraints presented by the wireless sensor platforms during operation. The results of this initial experimental validation will demonstrate the robustness of the system when a simple experimental specimen is considered. Accurate localization of damage, presented as high correlation values concentrated at the damaged positions, is accomplished even when experimental uncertainties and numerical modeling errors are present.

3.1 Experimental Setup

The beam is 274.3 cm long, 7.6 cm wide and 0.6 cm thick. Seven *iMote2* platforms are attached to the beam to measure acceleration responses in the direction parallel to the weak axis, placed at constant intervals of 38.1 cm measured from the base. Sensors are configured to have a sampling frequency of 280 Hz, corresponding to a cutoff frequency of 70 Hz. Three damage scenarios are independently examined using impact testing. Rather than damaging the structure, additional mass is placed in specified locations to change the dynamics of the structure. Thus, each damage scenario is simulated by attaching a steel bar with an equivalent weight of 1.50 kg placed at distances from the base of: 66.0 cm (D1), 134.6 cm (D2), and 189.5 cm (D3), respectively. Figure 3.1 and Figure 3.2 show a schematic diagram and photo of the experimental setup. Additionally Figure 3.3 shows a view of the sensor network distribution on the cantilevered beam.

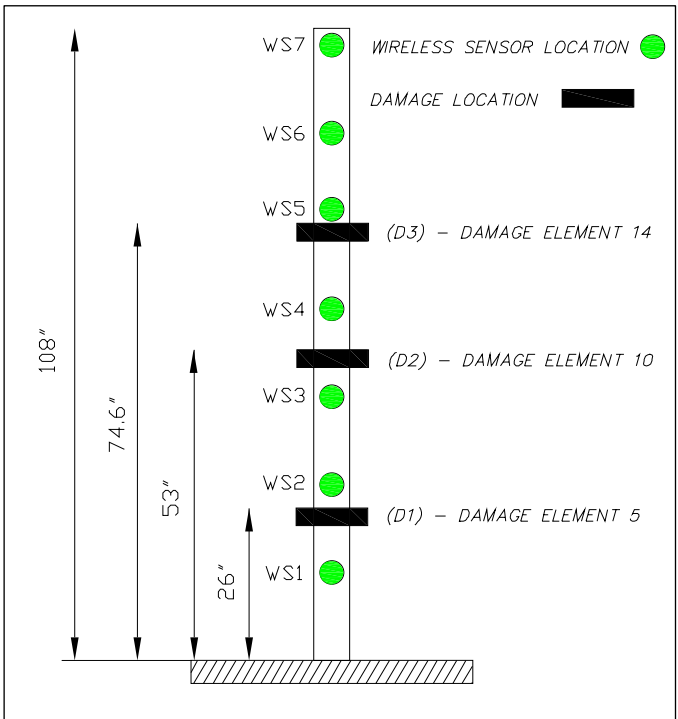


Figure 3.1 Diagram of cantilever beam test structure

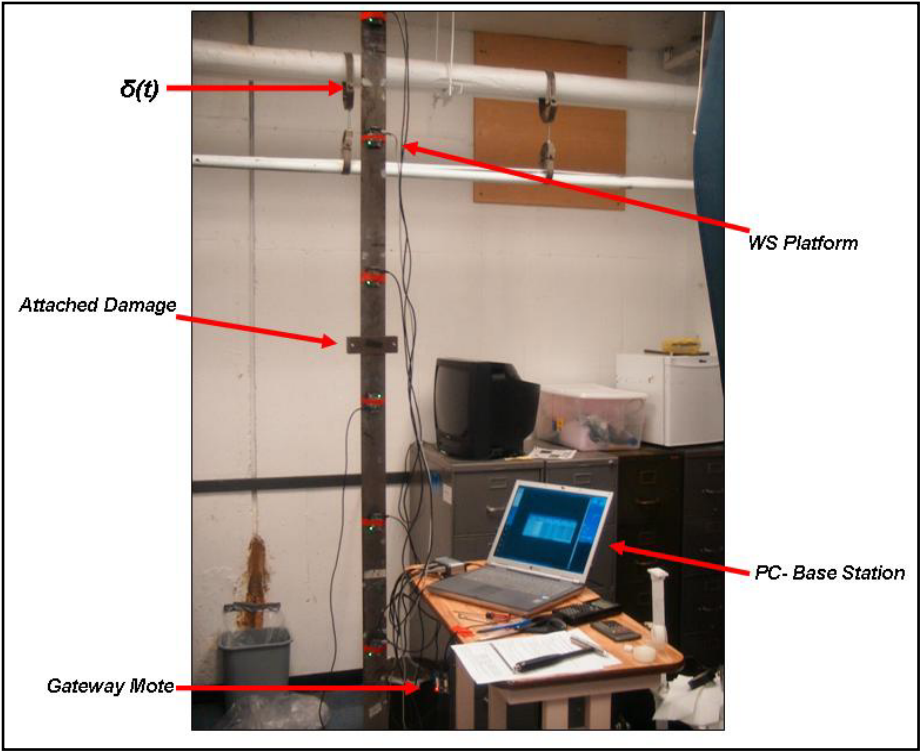


Figure 3.2 View of cantilever beam experiment

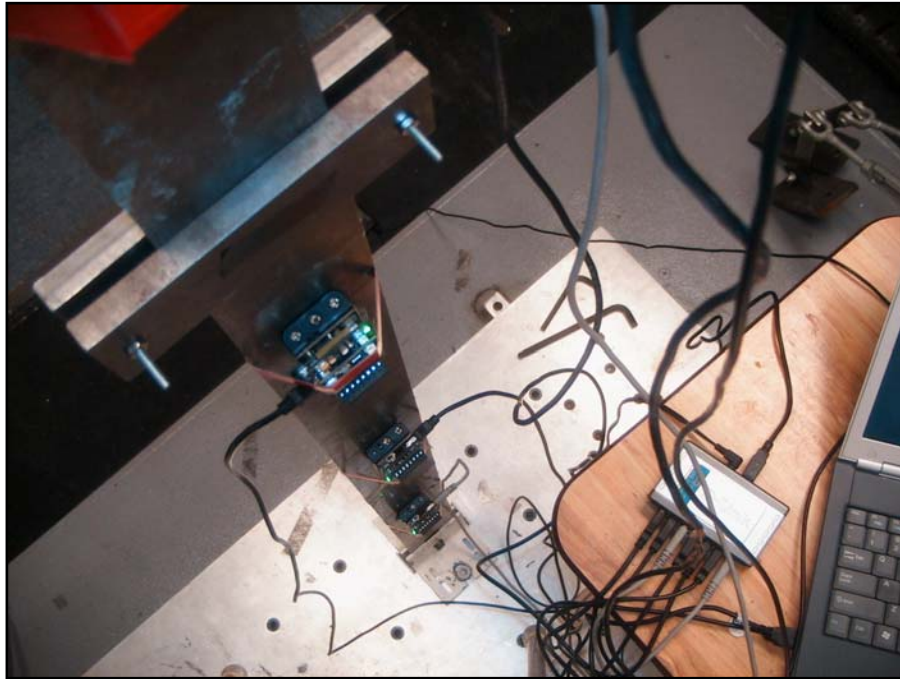


Figure 3.3 View of sensor distribution on cantilever beam experiment

3.2 Numerical Model

A numerical model is developed to yield analytical values of the healthy and damaged structures' natural frequencies for later correlation calculations needed for the DLAC technique. The model employs 2D Bernoulli beam elements with transverse and rotational degrees of freedom (DOF), producing a consistent mass matrix finite element model with 20 elements and 42 global degrees of freedom (see Figure 3.4). Boundary conditions assume a perfect cantilever support. Using the numerical model, 20 analytical damage scenarios are generated. Analytical damage is produced in the model by increasing the density in the damaged element to represent a mass increase.

Table 3.1 Analytical natural frequencies (Hz)

Mode	Healthy	D1	D2	D3
1	0.6564	0.6555	0.6443	0.6200
2	4.1133	4.0105	3.7649	4.0026
3	11.5180	10.6192	11.4581	10.7937
4	22.5710	20.8768	21.0991	22.3574
5	37.3160	36.1469	36.8913	36.1677

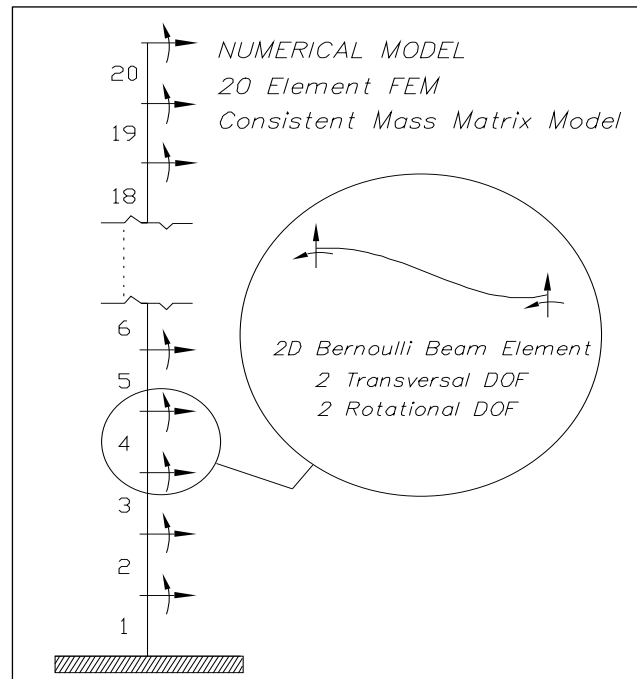


Figure 3.4 Cantilever beam finite element model

The assumed amount of mass added at each element is only 67% (1.00 kg) of the true experimental value of the added mass (1.50 kg). The eigenproblem is solved to obtain the healthy natural frequencies and a sensitivity matrix containing information about the first five bending natural frequencies for each of the 20 damage locations on the beam model. Analytical natural frequency results for healthy and damaged cases are given in Table 3.1. Each experimental damage scenario is associated with elements 5 (case D1), 10 (case D2) and 14 (case D3) in the model. Therefore, the highest DLAC values are expected to be concentrated around these positions.

3.3 Experimental Results

The first experimental test is performed to identify the healthy natural frequencies of the beam. A hammer strike is applied along the weaker bending axis of the beam to approximate an impulse response and to ensure a sufficiently broadband excitation.

Table 3.2 Experimental healthy natural frequencies (Hz)

Mode	1	2	3	4	5
ω_n	0.5381	4.0240	11.4705	22.5506	37.4316

The first five healthy natural frequencies, shown in Table 3.2, were determined by averaging the results obtained from each of the smart sensors and incorporated into the java tool to perform the DLAC computations.

The observed differences between the analytical and experimental healthy natural frequencies can be explained due to assumptions in the analytical model. Boundary conditions, homogeneous distribution of density and constitutive laws, and disregarding the mass of sensor platforms are the most important causes for those discrepancies. However, later results demonstrated that the DLAC algorithm is reliable and robust to modeling errors even when these differences are large (Clayton, 2006). In this case, the errors ranged from 18% in the fundamental mode to 0.3% in higher modes.

The damage scenario experiments are performed to test the distributed SHM system. Mass is attached to the beam and impact testing is used to excite the structure for each of the damage scenarios. For illustrative purposes, Figures 3.5, 3.6 and 3.7 provide representative output of three wireless sensor platforms under the three damage scenarios already explained. In each figure an acceleration time record and corresponding power spectral density function is shown. The curve fit functions are also presented showing the exact natural frequency locations.

The results reported by the wireless sensor network are provided in Figures 3.8, 3.9 and 3.10. The corresponding identified natural frequencies (in Hz) and DLAC measurements are presented for each damage scenario. Recall that the experimental damage cases D1, D2 and D3 are associated with elements 5, 10 and 14, respectively. From these results it is clear that the highest DLAC values correspond directly to the damage location for this simple beam structure.

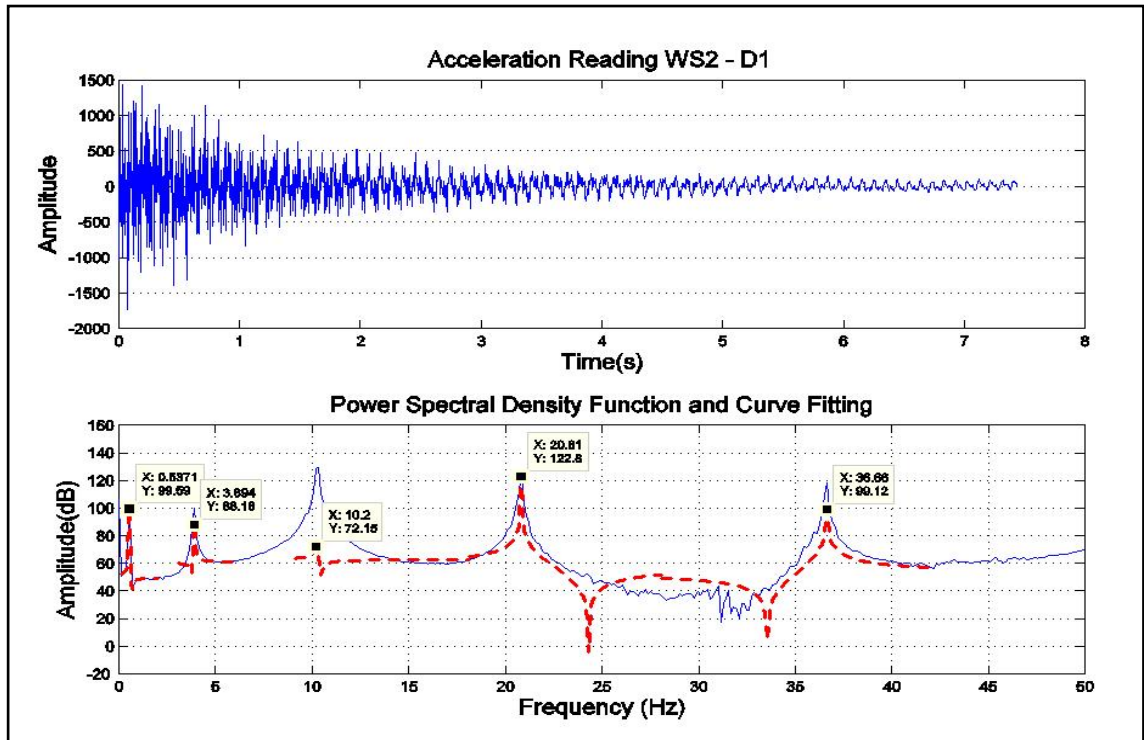


Figure 3.5 WS2 acceleration record and corresponding PSD under damage scenario D1

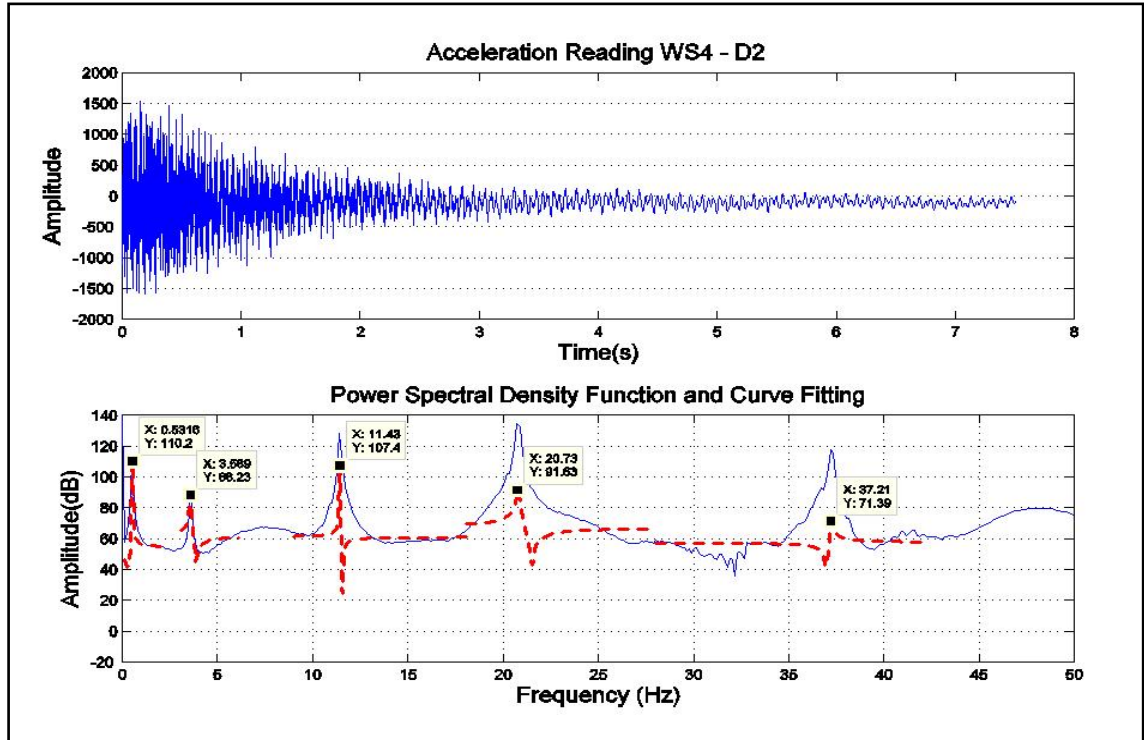


Figure 3.6 WS4 acceleration record and corresponding PSD under damage scenario D2

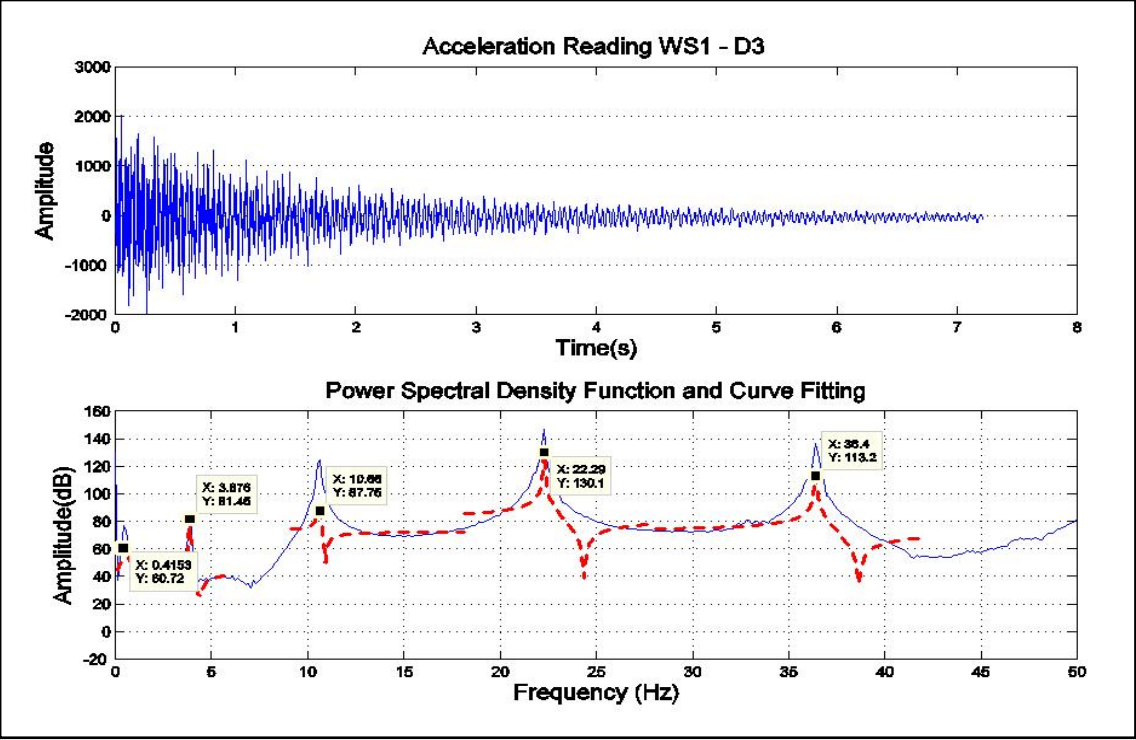


Figure 3.7 WS1 acceleration record and corresponding PSD under damage scenario D3

Despite the accuracy of this approach in localizing damage here, some of the sensors do report similar DLAC values in the final damage scenario (**D3**). This outcome appears to be due to the pattern in the frequency change being similar for two damage scenarios. Using more frequencies in the DLAC method would likely correct this error, but at this time this study is would be outside the bandwidth of the sensors. However, this method is found to be robust to the level of damage assumed for DLAC determination, requires only a few modes for implementation, and has not been found to result in false negatives; locations indicating high levels of correlation do include the damage location.

Mode	WS1	WS2	WS3	WS4	WS5	WS6	WS7
1	0.5506	0.5374	0.5402	0.5316	0.5371	0.5427	0.5392
2	3.9043	3.8902	3.8977	3.8564	3.7678	3.8488	3.9012
3	10.2473	10.2779	10.2714	10.2744	10.0707	10.3217	10.2533
4	20.7641	20.8096	20.7964	20.8470	20.4038	20.7546	20.7751
5	36.6415	36.6396	36.6048	36.6785	35.9797	36.5919	36.6570

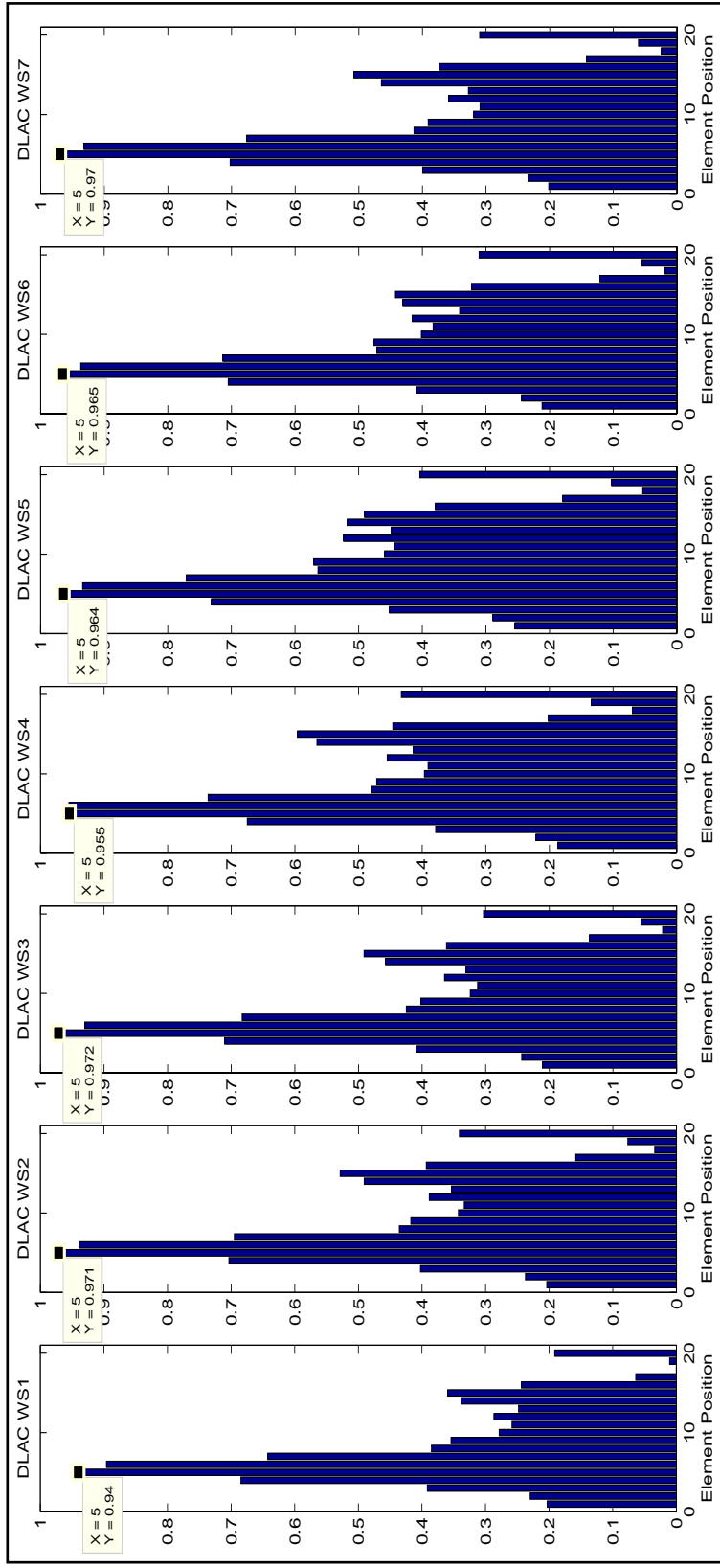


Figure 3.8 DLAC results for element position # 5

Mode	WS1	WS2	WS3	WS4	WS5	WS6	WS7
1	0.5498	0.5393	0.5386	0.5318	0.5353	0.5420	0.5379
2	3.6042	3.6241	3.6343	3.5979	3.7358	3.5478	3.6284
3	11.4766	11.4127	11.4758	11.4310	11.2721	11.3961	11.4565
4	20.7626	20.7606	20.7952	20.7798	20.4008	20.7528	20.7586
5	37.2342	37.2030	37.2573	37.2568	36.6449	37.1650	37.2391

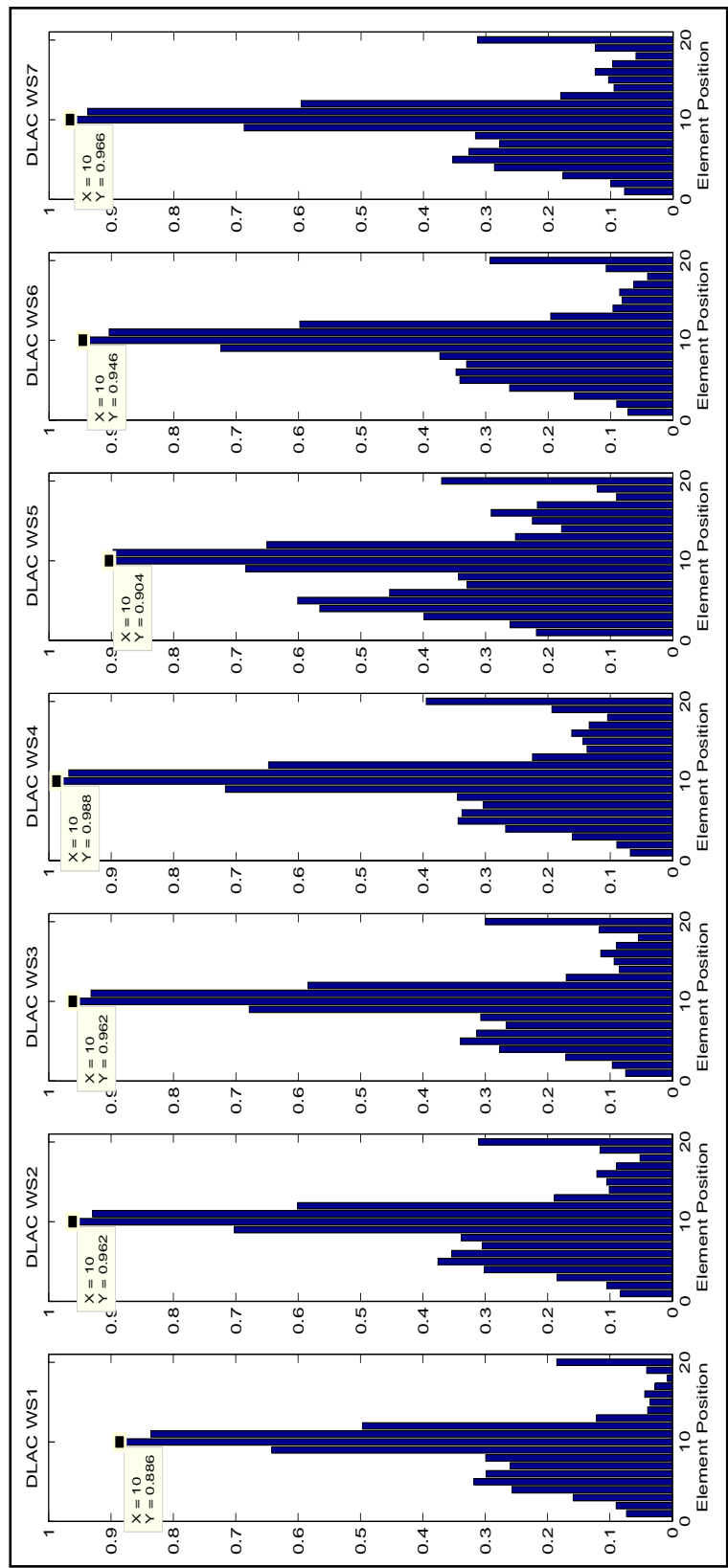


Figure 3.9 DLAC results for element position # 10

Mode	WS1	WS2	WS3	WS4	WS5	WS6	WS7
1	0.4767	0.4998	0.5030	0.5167	0.4806	0.4925	0.5101
2	3.8829	3.8889	3.9201	3.8785	3.8450	3.9297	3.9071
3	10.6125	10.6045	10.5549	10.6421	10.4151	10.5883	10.6263
4	22.2777	22.2284	22.2484	22.2936	21.8712	22.2304	22.2407
5	36.4255	36.3849	36.4066	36.4745	35.8035	36.3518	36.4494

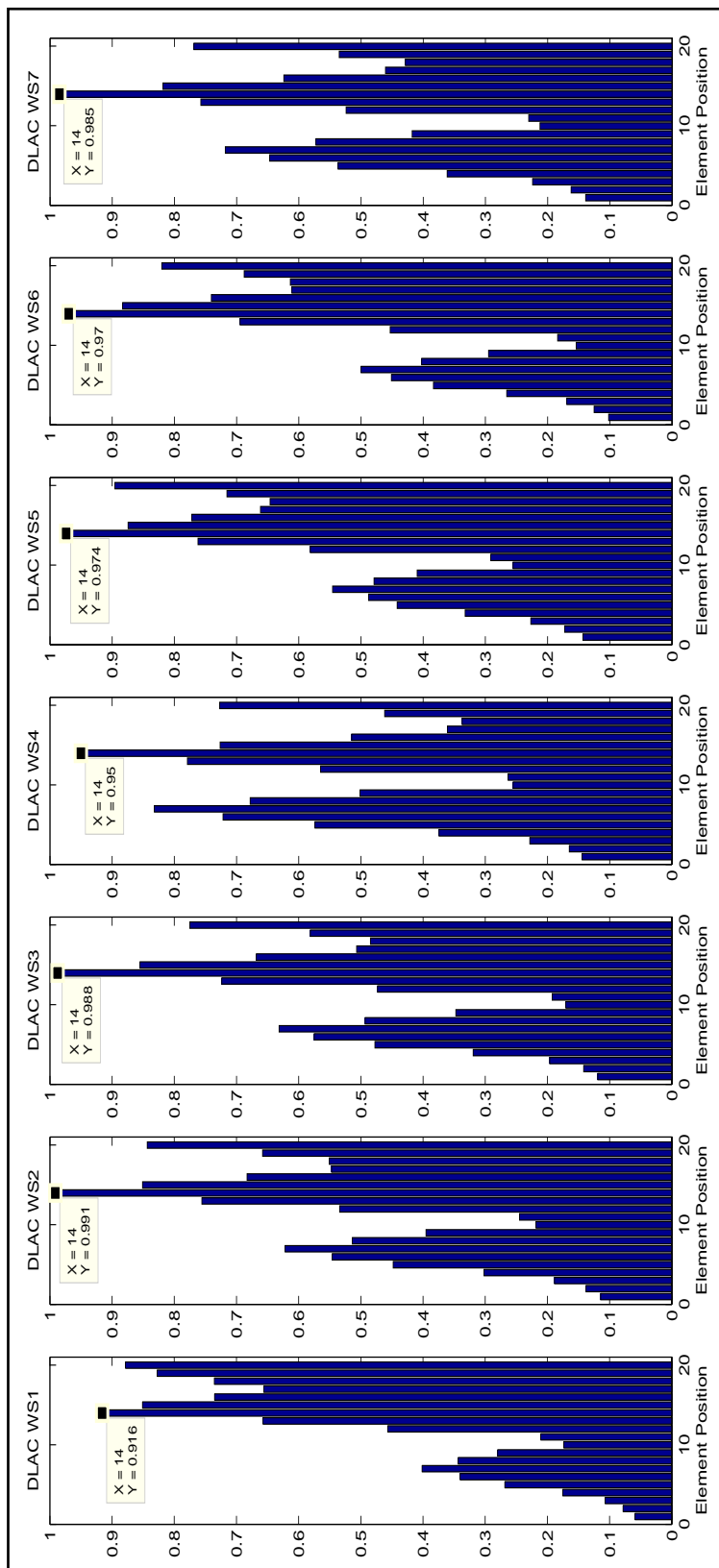


Figure 3.10 DLAC results for element position # 14

3.4 Summary

This chapter is focused on a discussion of the approach and results of an initial experimental validation of the proposed distributed damage detection system. The system is deployed and validated in a simple cantilevered beam using a network of seven wireless sensors. A damage detection pattern, required by the correlation-based damage detection technique, is developed based on a finite element approach. Three different damage scenarios are tested. The damage location is successfully identified in each damage scenario assuming an arbitrary damage level for developing the DLAC coefficients.

Chapter 4

Truss Structure Experiment

In this chapter a second experimental validation of the proposed distributed damage detection system is performed using a wireless sensor network deployed on a significantly more complex structure. A 3D steel truss structure is selected as the second experimental model (Clayton, 2002; Gao, 2005; Nagayama, 2007). This model is housed in the Smart Structure Technology Laboratory (SSTL) at the University of Illinois at Urbana-Champaign (see Figure 4.1) and has been the subject of several SHM studies in the past. Due to the geometrical complexities presented in this structure a more realistic structural response including bi-directional bending and torsion vibration is measured.



Figure 4.1 3D truss test structure

Therefore, frequency identification is much more challenging than in the beam. However, the results of this experimental validation will demonstrate the robustness of the system even when a complicated structure and numerical imperfections are considered. Damaged locations are detected and localized as high correlation measurements concentrated around the potential damage zones. Additional off-line and numerical analysis are also performed to test the reliability of the method under other damage scenarios and experimental uncertainties.

4.1 Experimental Setup

The specimen is 5.6 m long, has 14 bays each 0.4 m in length and depth, and rests on four rigid supports. Two of these supports, located at one end of the truss, are pinned and are able to rotate freely with all three translations constrained. The other two supports, located at the other end of the truss, have rollers and are able to translate only in the longitudinal direction of the truss. Each of the truss members has a tubular cross section with an inner diameter of 1.09 cm and outer diameter of 1.71 cm and can be removed or replaced for simulating damage without disassembling the entire structure.

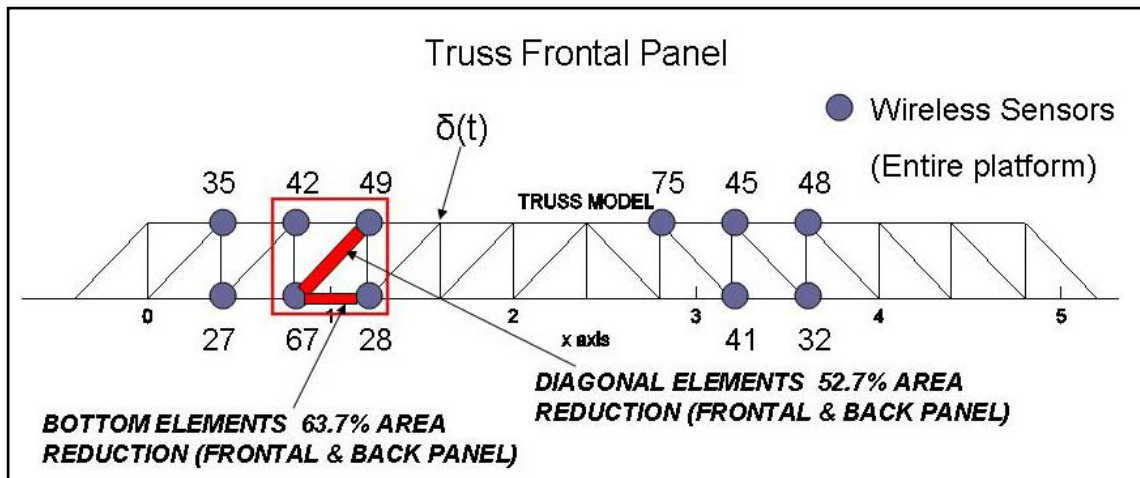


Figure 4.2 Truss experiment setup

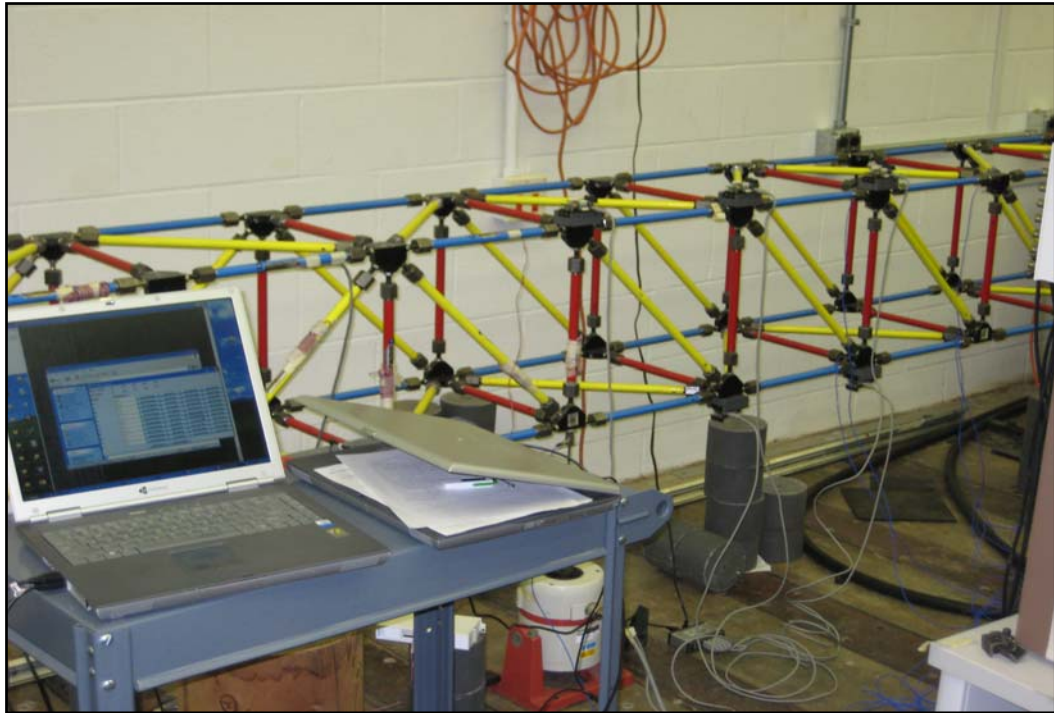


Figure 4.3 Truss experiment setup

In our implementation a network of eleven *iMote2* wireless sensor platforms is deployed on the front panel of the truss as indicated in Figure 4.2. Sensor boards are configured to measure vertical acceleration data with a sampling frequency of 560 Hz which corresponds to a cutoff frequency of 140 Hz. Sensors are oriented in the vertical direction to focus on measuring bending modes of the structure and identification numbers are defined for later interpretation of the data (see Figure 4.3 and Figure 4.4).

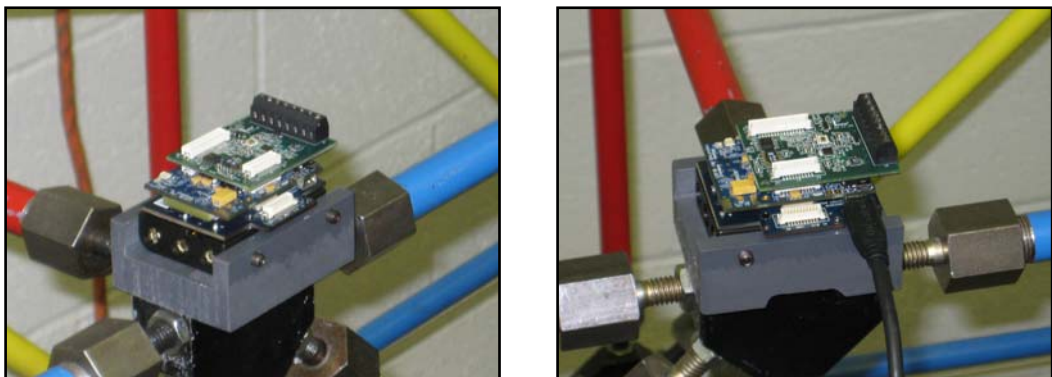


Figure 4.4 Two views of the sensor setup

4.2 Numerical Model

A numerical model is developed to produce the necessary frequency change vectors for the DLAC computations. 3D Bernoulli beam elements are used with transverse, rotational, torsion and axial degrees of freedom to produce a consistent mass matrix finite element model with 160 elements and 336 global degrees of freedom. The finite element model is shown in Figure 4.5. Boundary conditions are modeled in agreement with the actual boundary conditions of the truss. Three translational and three rotational degrees of freedom are defined for each structural node and an additional mass of 1 kg is lumped at every translational DOF to account for inertial effects introduced by the steel joints. An effective experimental damage scenario is performed by replacing four members of the third central bay on both the front and rear truss panels as shown in Figure 4.2 and Figure 4.5. Diagonal members are replaced with members having a reduced area of 52.7% of the original and bottom chord elements are replaced with members having a reduced area of 63.7 % of the original.

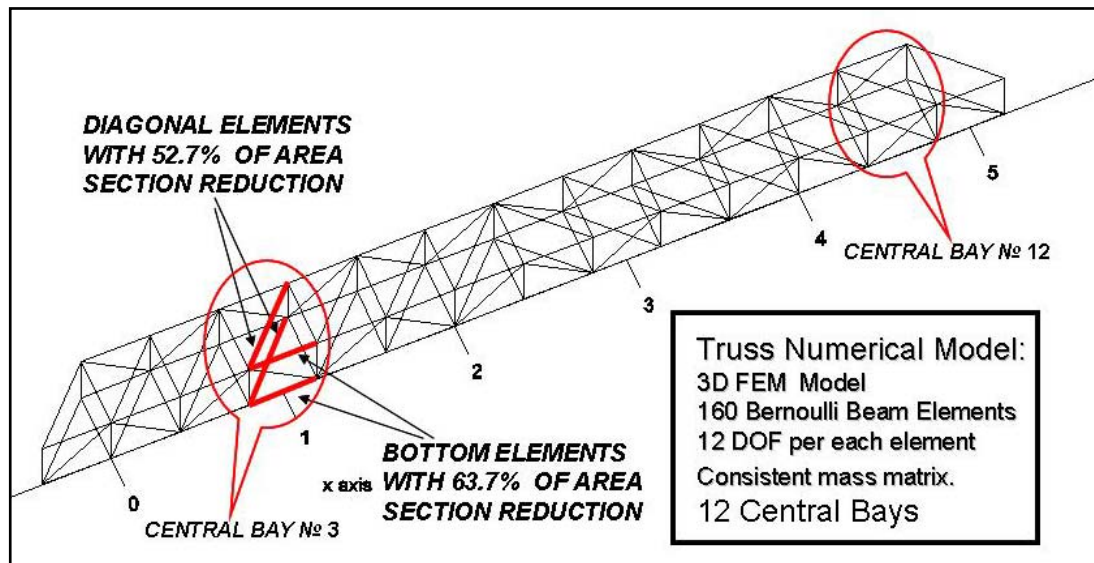


Figure 4.5 Truss finite element model

Table 4.1 Analytical natural frequencies (Hz)

Mode	1	2	3	4	5
Healthy	19.88	38.31	66.26	67.17	92.25
Damaged	19.19	38.35	63.58	66.30	90.96

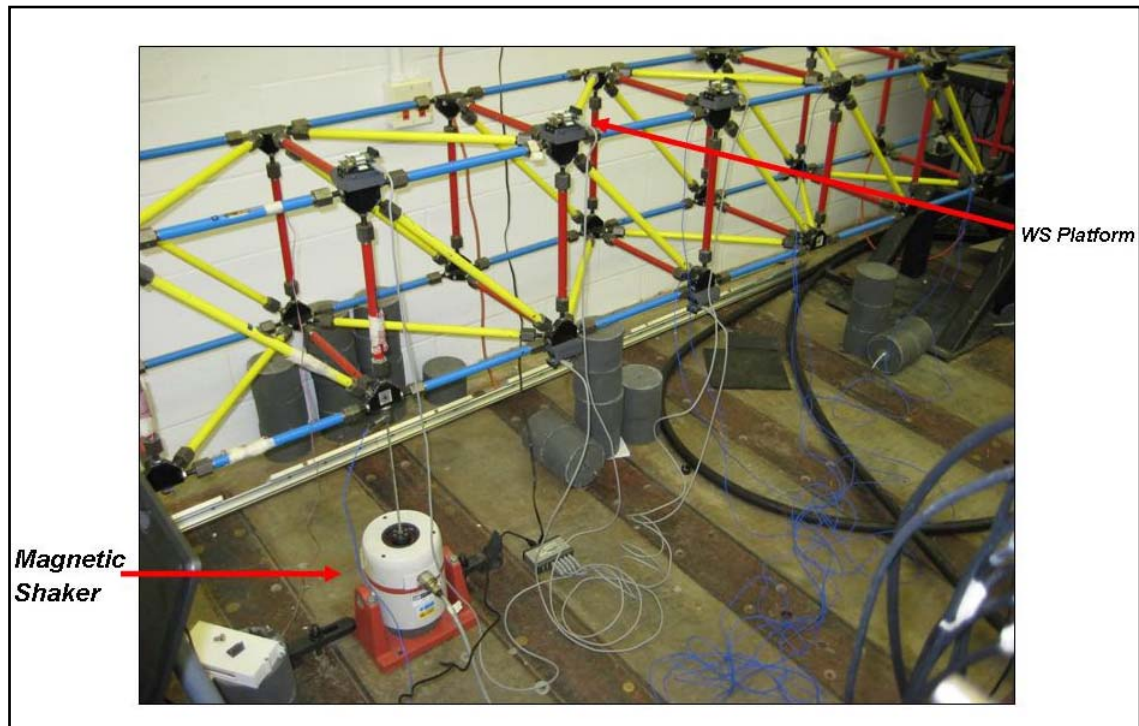
Damage patterns corresponding to a reduction in the area of the diagonal and bottom elements in each of the 12 central bays are then reproduced in the analytical model. Here the actual experimental damage is applied by modeling the same section reduction. Therefore, for the experiments a damage hypothesis identical to the actual damage is used to produce a damage detection pattern for correlation comparisons. However, modeling errors are included in the analysis as the analytical model of the truss has not been updated to reflect the healthy condition of the structure. Analytical natural frequency results for healthy and damage cases are depicted in Table 4.1. A frequency change vector that includes the first five bending natural frequencies over each of the 12 damage scenarios is calculated. Note that according to the true damage patterns, the highest DLAC values are expected to be concentrated around to the third bay due to the presence of damage.

4.3 Experimental Results

Modal identification is initially performed to accurately capture the dominant longitudinal bending modes in the system for model validation. The eigensystem realization algorithm (ERA) (Juang and Pappa, 1985) is used here to perform the modal identification using forced response data. An electromagnetic shaker that can generate a maximum force of 20 lb and having a bandwidth of 5-9000 Hz is used to vertically excite the structure, as shown in Figure 4.6. A command input characterized by a band-limited white noise up to 256 Hz is applied to this shaker. Output data is acquired using six wired accelerometers mounted on the front panel, each measuring vertical response data with a sampling frequency of 512 Hz. Additionally, input force measurement is obtained using a force transducer, located between the shaker and the structure. This test is performed with the full set of eleven wireless sensors attached to the truss to ensure that the mass distribution is identical before and after damage is applied to the system.

Table 4.2 Experimental healthy natural frequencies (Hz)

Mode	1	2	3	4	5
W_n	20.65	41.49	64.59	69.41	95.51

**Figure 4.6 View of Magnetic Shaker**

System transfer functions are obtained and converted to impulse response functions. The ERA is applied to the impulse response functions to detect the first five dominant frequencies. The natural frequencies associated with the first five dominant bending modes of the healthy structure are given in Table 4.2.

These values are incorporated in the java tool that computes the final DLAC coefficients. Experimental and analytical natural frequency values showed small differences ranging from 7% to 2% and due to numerical assumptions on the analytical model. Additionally, note that these values are not obtained using the wireless sensors, and thus some additional experimental errors are introduced, demonstrating the robustness of the technique.

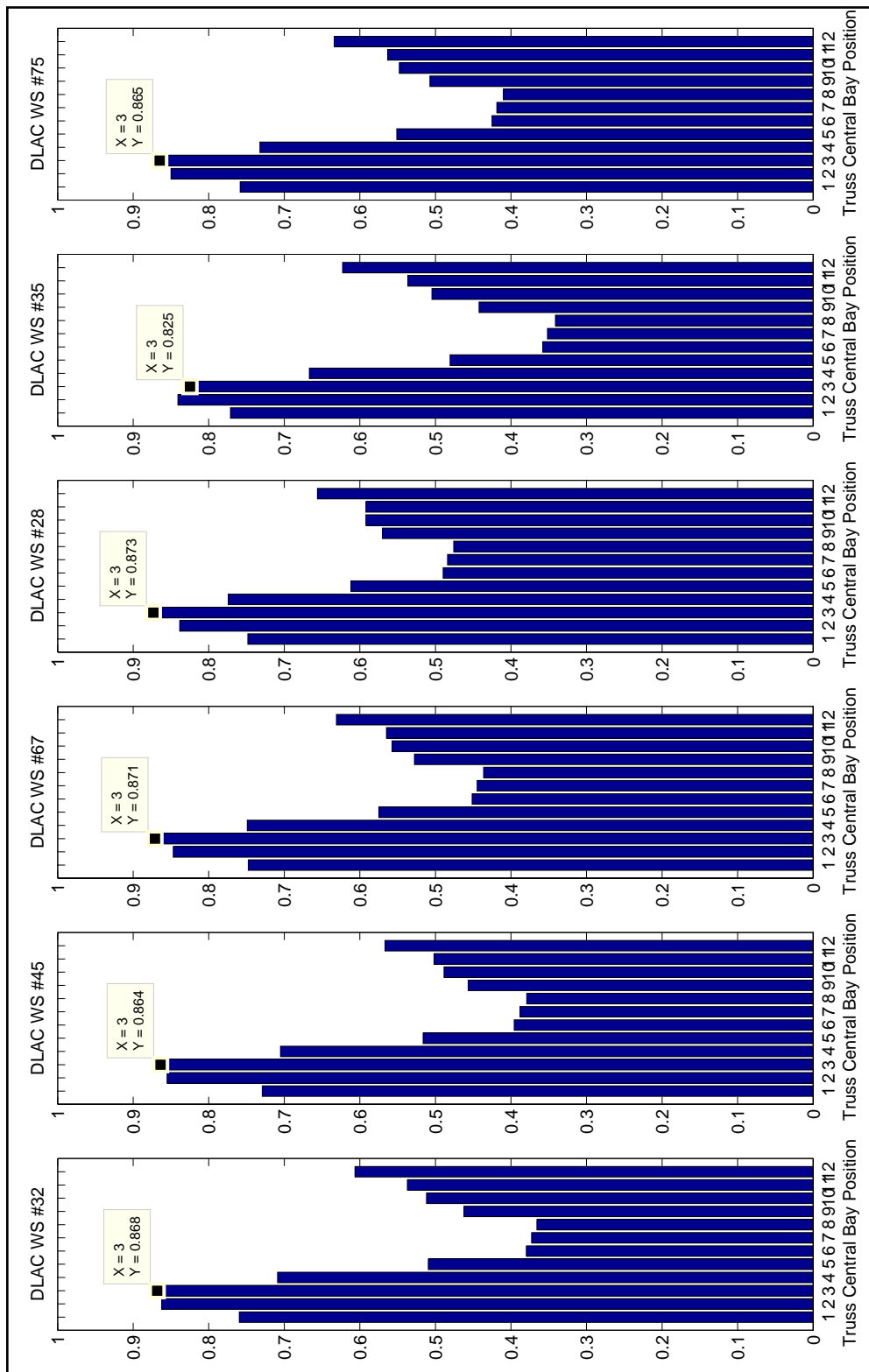


Figure 4.7 DLAC results for truss bay # 3

Table 4.3 Identified natural frequencies (Hz)

Mode	WS #32	WS #45	WS #67	WS #28	WS #35	WS #75
1	20.2718	20.2795	20.1952	20.1685	20.3122	20.2254
2	41.3708	41.4002	41.2871	41.2315	41.2998	41.2947
3	63.0427	63.1657	63.0138	63.0467	63.1021	63.0198
4	67.7883	67.8858	67.6658	67.6792	67.7284	67.6820
5	94.8858	95.0803	94.8184	94.7336	94.8865	94.8080

Damage is then introduced in the experimental truss by exchanging the indicated members to validate the proposed distributed SHM system. Impact testing, represented as $\delta(t)$ in Figure 4.2, is employed to perform the validation by disconnecting the electromagnetic shaker and applying a hammer strike perpendicular to the longitudinal axis of the truss. Due to malfunctions in the drivers of the accelerometers that were provided by the manufacturer, only 6 of the 11 sensors reported acquisition of raw data during the experiment. The results obtained by the SHM system are provided in Table 4.3 and Figure 4.7. The results indicate the highest DLAC values are located at the damaged position (third bay). Here it is demonstrated that the approach is able to localize damage correctly even though modeling errors are present in the frequency change vectors.

4.4 Off-Line Experimental Results

Additional off-line analysis is conducted using the experimental data to study the capabilities of the technique when the assumed damage pattern is significantly different than the actual damage pattern. Various assumed damage patterns are used in these off-line studies to evaluate the robustness of the approach. Here, additional assumed damage levels are considered and the experimentally obtained values for the healthy and damaged natural frequencies are used for DLAC correlation. Here each analytical damage scenario is simulated by replacing the set of 6 members in each bay with elements having a reduced area, as shown in Figure 4.8. To generate the frequency vectors associated with the damage hypotheses, the analytical model is modified by using elements with 25% and 50% reductions in the elemental cross-sectional areas of

damaged members. Analytical natural frequency results for healthy and damaged cases are also depicted in Table 4.4. Because the damage in the experimental structure is in the third bay, the highest correlation results are expected to be concentrated around to that position. The DLAC results of this off-line study are shown in Figure 4.9 and Figure 4.10. The highest correlation values are concentrated between the first and third bay. Thus, even though the hypotheses are very different than the actual damage, the damage zone is determined with only five natural frequencies. The results for the case considering a 25% reduction in area (Figure 4.9) show a symmetric pattern in the DLAC values corresponding to the three first and three last bays. This tendency can be explained by the nearly perfect symmetry of the structure. Therefore, DLAC approach is shown to be capable of detecting the most likely damage zones. Perhaps, if additional information is needed, this low power approach would be used for detecting damage zones, and a secondary level of analysis that requires more resources would be used to follow up.

Figure 4.8 Truss finite element model

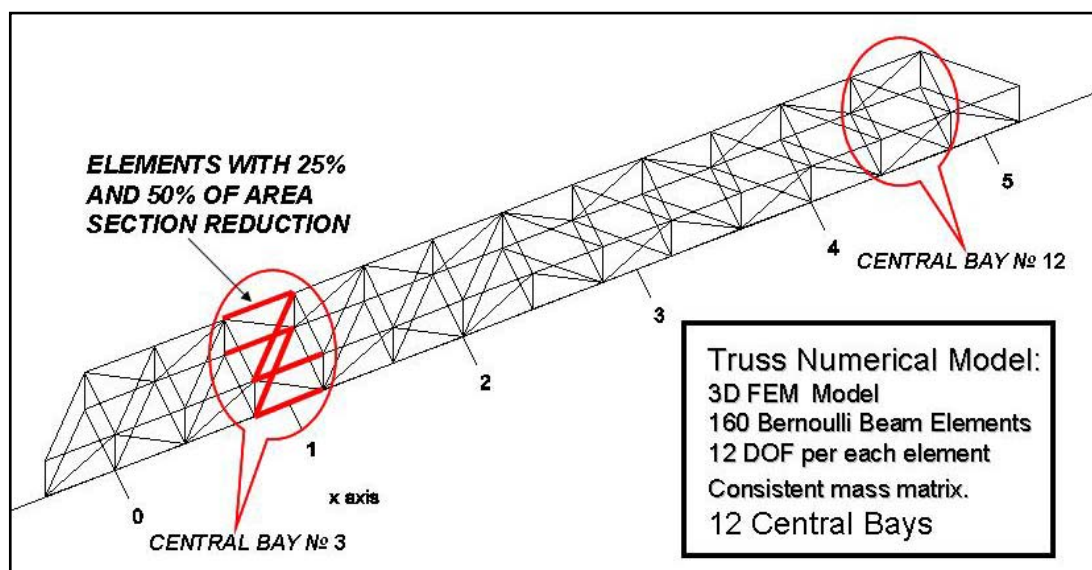


Table 4.4 Analytical natural frequencies (Hz)

Mode	1	2	3	4	5
Healthy	19.88	38.31	66.26	67.17	92.25
Damaged 25%	19.70	38.23	66.28	66.36	91.99
Damaged 50%	19.30	38.01	64.72	66.29	91.28

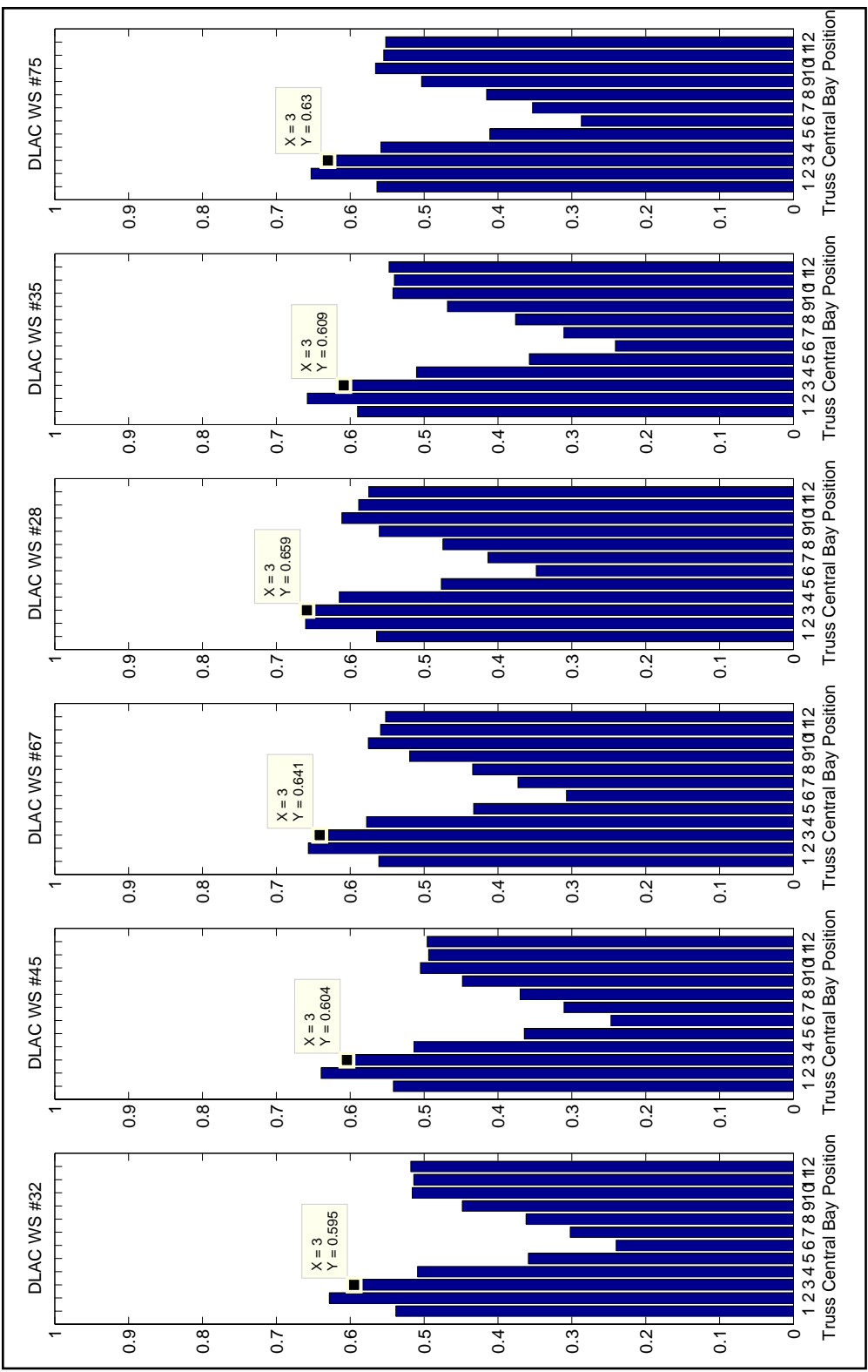


Figure 4.9 DLAC results for truss bay # 3 under 25 % of area section reduction

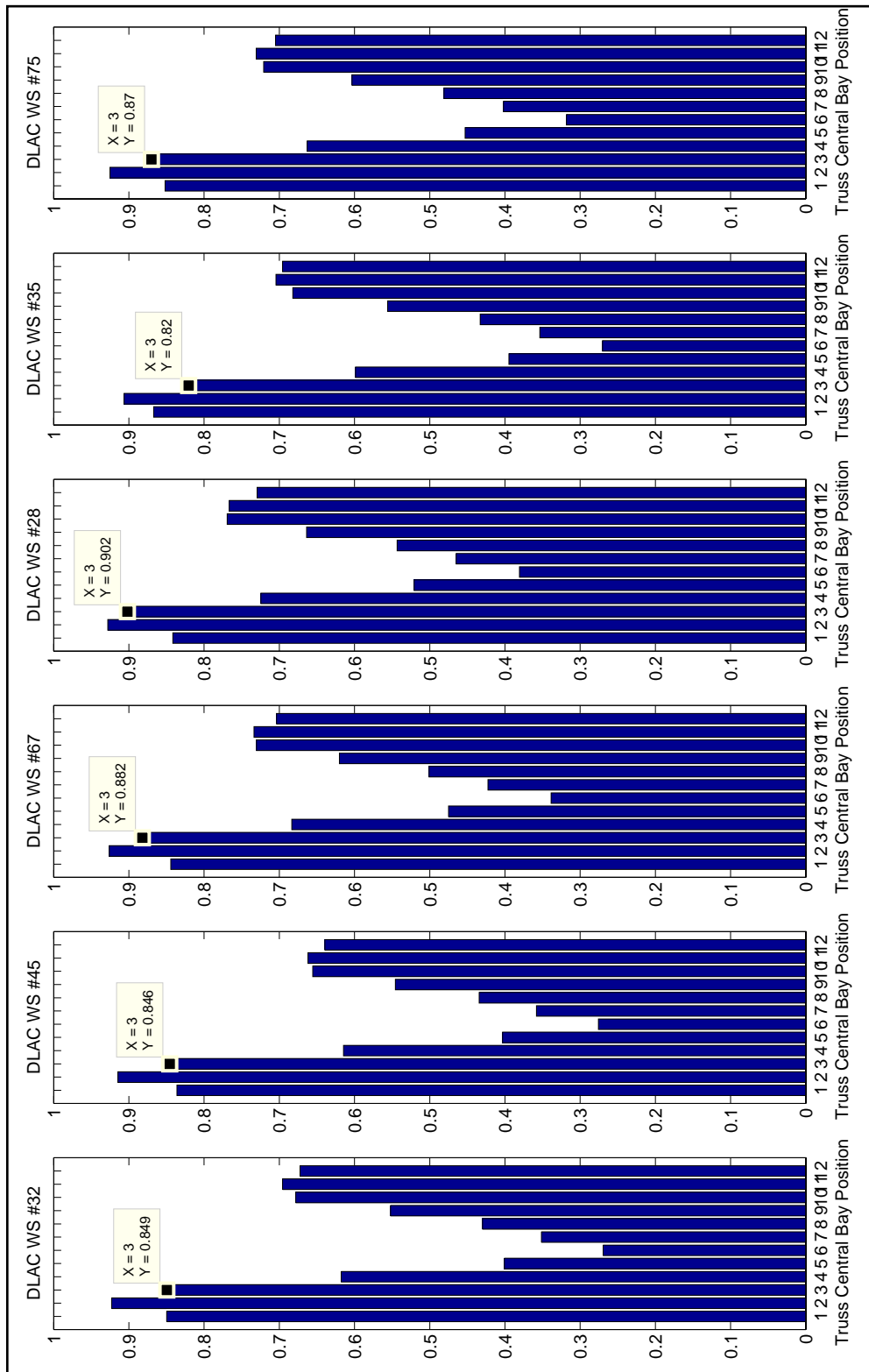


Figure 4.10 DLAC results for truss bay # 3 under 50 % of area section reduction

4.5 Additional Numerical Studies

Additional analytical studies are performed in this section to validate the robustness of the DLAC method under different damage locations. A simulation, using the analytical model, is implemented in MATLAB (MathWorks, 2006) to independently analyze two alternate damage positions with assumed damage levels corresponding to 25% and 50% reductions in the cross-sectional area. An equally spaced deployment of sensors is assumed in this study where the network of eleven sensor platforms is positioned along the frontal panel of the truss. The description of the cases considered is shown in Figure 4.11.

The conditions used in the actual experiments are simulated in these numerical studies. Therefore, a sampling frequency of 560 Hz and corresponding cutoff frequency of 140 Hz are defined for each sensor to measure vertical acceleration data. Thus, to produce accurate results, the simulation time step is set to 1/5600sec and resampling is applied to the output to generate raw data sensed at the appropriate sampling frequency. The input is generated by the use of a numerically generated impulse function, represented as $\delta(t)$ in Figure 4.11 to approximate the effect of impact testing.

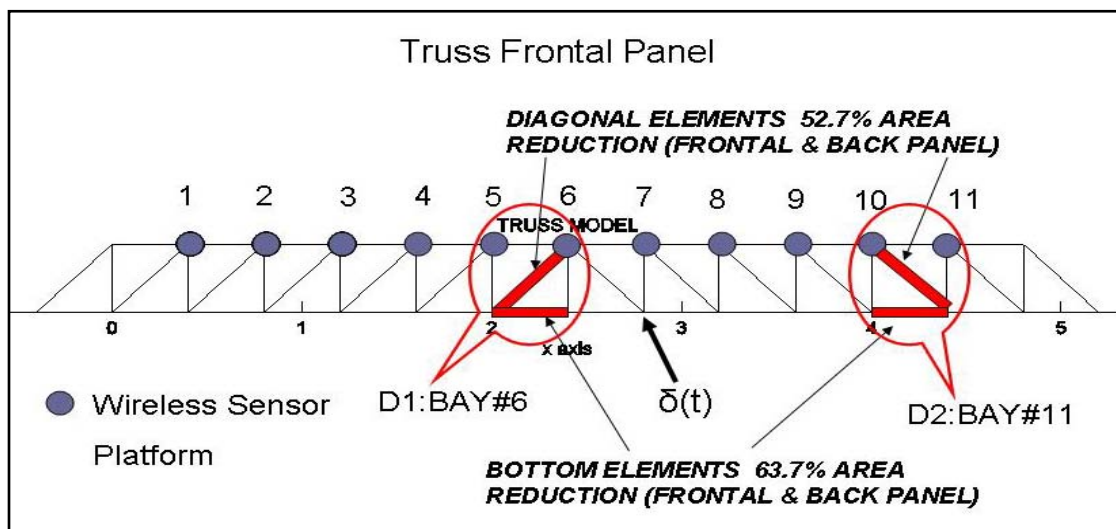


Figure 4.11 Numerical simulation setup

Physical uncertainties in the experimental model and data measurement errors involved in a true experiment are also simulated to produce *experimental* natural frequencies under more realistic conditions (Clayton, 2006). Sensor noise is considered, defined as a Bandlimited white noise with a magnitude of 10% of the standard deviation of the output signal. A non-homogeneous random distribution of elemental densities and elastic moduli among the truss members are included to represent modeling errors. The same data processing is used as in the experimental implementation, involving the curve fitting technique, is performed over the raw data. Consequently, numerical values for the *experimental* healthy and damaged natural frequencies are obtained in a range of 8-10% of the analytical natural frequencies. A typical acceleration time history and corresponding power spectral density function reported by one of the sensors is provided in Figure 4.12.

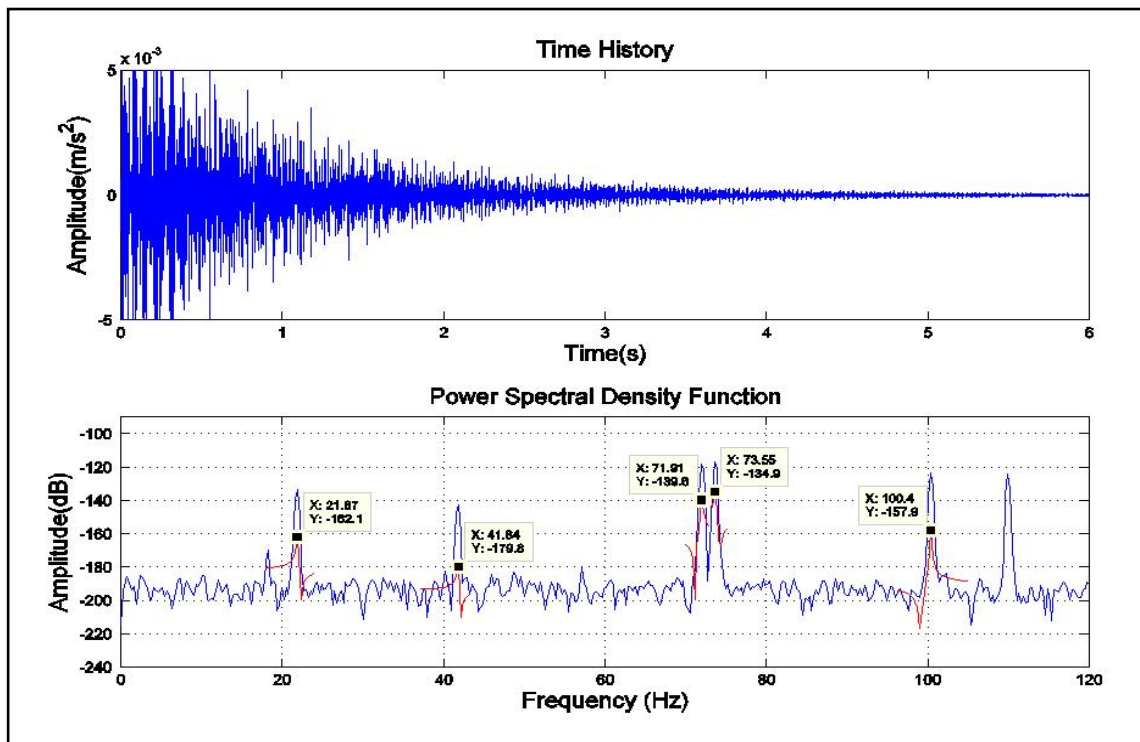


Figure 4.12 Typical acceleration time history and corresponding PSD function

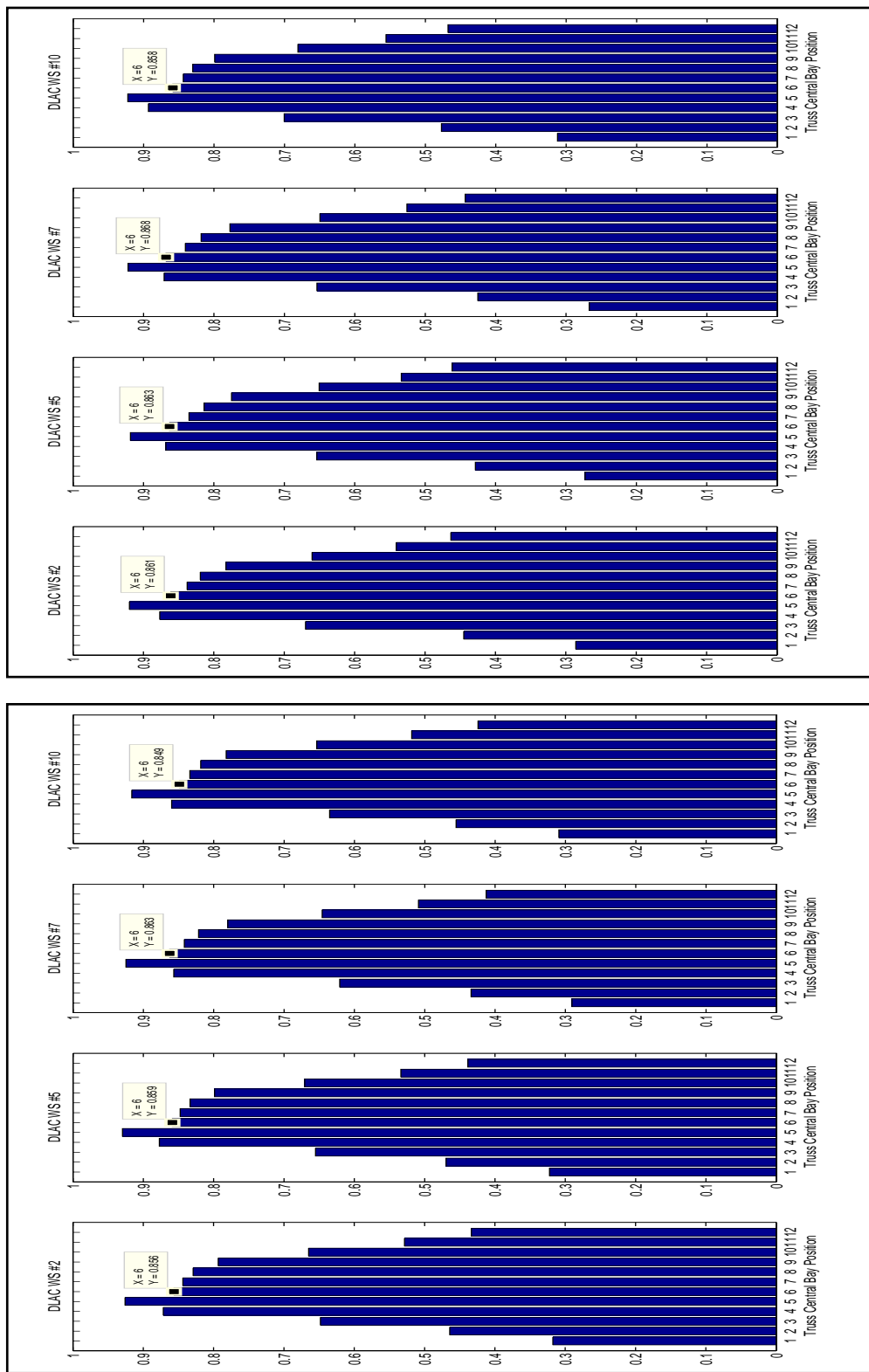


Figure 4.13 DLAC results for truss bay #6 under 25% and 50 % of area section reduction

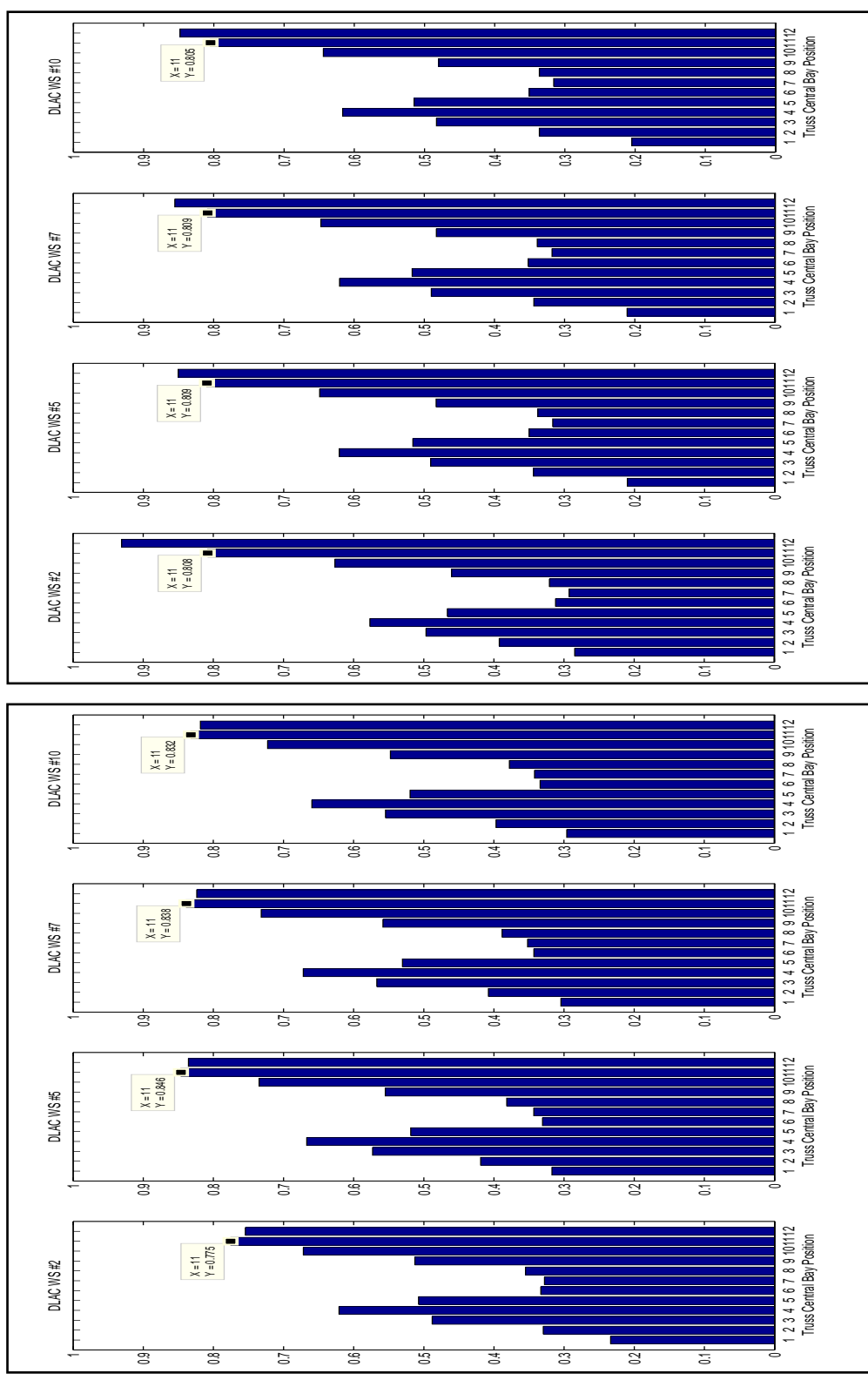


Figure 4.14 DLAC results for truss bay #11 under 25% and 50 % of area section reduction

Damage is induced under the same conditions and configuration as the true damage imposed on the truss. Each damage scenario, **D1** and **D2**, is associated with truss bays # 6 and # 11 respectively, as shown in Figure 4.11. Therefore, the highest correlation values are expected to be concentrated around the sixth and eleventh bay because damage is located in these positions.

Results depicted in Figures 4.13 and 4.14 show the calculated DLAC values. Four representative sensor outputs are shown for each damage case (25% damage assumption (left plot) and 50% damage assumption (right plot) shown in each figure). The results of the first case (**D1**) indicate that structural damage is concentrated between the fourth and sixth bays. In the second case (**D2**) the results indicate that structural damage is concentrated between the eleventh and twelfth bays. Therefore, both results are considered successful because the most likely damage zones have been detected with very different hypotheses than the actual damage and using only five natural frequencies. Thus, the results of the numerical studies are consistent with the experimental studies in detecting damage at different positions.

4.6 Summary

Chapter 4 focuses on a second experimental validation of the proposed distributed damage detection system. The system is deployed and validated on a 3D truss structure of considerable more complexity using a wireless sensor networks (WSN). A damage detection pattern, required by the correlation-based damage detection technique, is developed based on a finite element model. A real damage scenario is tested leading to successful results for all the network sensors. Additional numerical analyses using the experimental results along with additional numerical studies are presented to test the reliability of the proposed distributed algorithm under other damage locations and more realistic damage patterns. Results showed the potential offered by the DLAC method to determine the most likely damage zones in a real structure.

Chapter 5

Conclusions and Future Work

In this study a distributed SHM system using a correlation-based damage detection technique for implementation on a wireless sensor network has been proposed and validated. First, the need for distributed implementations was highlighted. The distributed approach used in this system was then formulated and its entire implementation thoroughly described. Finally, successful results of an experimental validation on two structures of differing complexities were presented. The following paragraphs summarize the most meaningful conclusions of the present study.

The importance of wireless sensor technology and smart sensor platforms in the structural health monitoring field has been highlighted. The attractive features of these systems include:

- Wireless transmission capabilities will reduce the cost associated with installation and will increase the possible number of sensors that may be used. Additionally, the flexibility of the damage detection system and reconfigurable nature can be exploited.
- On-board processing capabilities can be exploited to reduce the communication overload and thus the power needs of these systems. However, even though wireless sensors appear as a promising tool, some hardware constraints still limit their applicability and scalability for dense deployments under common centralized SHM implementations.

A new distributed damage detection system has been formulated and experimentally validated in situ. The system, based on the Damage Location Assurance Criterion (DLAC) adopted for performing damage detection, was implemented in four steps. Data

acquisition, data processing, data transmission and final damage localization implementation steps were described and discussed. The advantages of this system include:

- The proposed method is simple and completely distributed, and thus is scalable to any size structure or wireless sensor network.
- The method is effective for detecting damage in same classes of structural systems.
- The damage detection technique is robust to errors in the numerical model, but is more effective when several modes can be identified.
- Effective partitioning in the data aggregation flow was achieved leading to a significant reduction in the amount of transmitted data, latency and energy usage in the system. A 98.8% of communication load was achieved because only a set of reduced number of parameters are transmitted to the base station.
- A statistical evaluation of the latency demonstrated that distributed implementation was able to achieve latencies 64.8% lower than those of a centralized approach.
- Energy usage reduction of almost 70.0% lower than that used in a centralized approach was also achieved.

Experimental validation of the system using a wireless sensor network has been performed on two experiments of increasing complexity. The results include:

- Initial experimental validation of the proposed distributed damage detection system was performed on a simple cantilevered beam structure using a network of seven wireless sensors. The experimental results indicated that the proposed

correlation-based algorithm was extremely robust to detect damage even when experimental uncertainties and numerical errors were present during the validation. Damage was detected in three scenarios with high correlation values.

- Experimental validation was also performed on a 3D truss structure and a network of six working wireless sensors. The purpose of this second validation was to test the damage detection system under more realistic conditions and complicated dynamics than the previous experiment. The initial experiment used the same damage detection pattern as the actual imposed damage. The results indicated a successful damage detection study which yielded high correlation values at the expected damaged location. The success of the proposed damage detection system was evidenced even though numerical modeling errors and experimental uncertainties were present.
- Further off-line studies were performed using the experimental results. Post-processed data, including natural frequencies, were used with the DLAC method to investigate the abilities of this approach when the assumed damage level is not equal to the true damage level. The results successfully yielded the detection of zones corresponding to the actual damaged location. In these results, damage was detected as a concentration of high correlation values around the expected damage location. Therefore, the method's success in precisely detecting the damage location is influenced somewhat by the selection of the assumed damage pattern. However, the method is still very capable of detecting a zone with the highest correlation values that includes the true damage location.
- Additional numerical studies were also conducted to test the DLAC technique under other damage cases. Experimental uncertainties and different damage patterns were assumed in this numerical evaluation. The results demonstrated that the DLAC method is suitable for determination of the most likely damage zones.

- Due to its low power needs, this damage detection system would perhaps be best employed as a first stage damage detection technique to be followed by a more powerful method focusing on localizing and quantifying damage more precisely.

The present work has shown a successful implementation and corresponding validation for a distributed damage detection system using the DLAC damage detection technique. Experimental results under more realistic conditions demonstrated that the DLAC methodology can be used most appropriately as a preliminary damage detection technique by localizing potential damage zones. However, some remaining constraints must be addressed to expand its applicability under realistic conditions. A set of proposed research goals in pursuing this objective are summarized:

- Analysis of the reliability of the DLAC method based on more realistic and more complicated structural configurations.
- Analysis of the influence of reduced frequency content perturbation in the correlation measurements.
- Analysis of the influence of numerical imperfections or modeling errors in the idealization of the damage detection patterns.
- A statistical evaluation to appropriately select the most effective damage patterns for the correlation measurements.

Although the system proposed here is effective for some classes of structures, it will not be useful in all structures or conditions. More robust damage detection techniques, capable of not only localizing but also of quantifying structural damage, must be also pursued. However, accurate detection and quantification of structural damage will usually demand excessive communication exchange, requiring advances in WSNs due to current hardware limitations. Therefore, research is still needed to ensure systems that are capable of performing damage detection and quantification in near real-time. Ideal

solutions will likely involve a combination of distributed and partially centralized implementations without involving large amount of data to be transmitted. The following bullets summarize some research requirements to be considered for such future implementations:

- The development of systems capable of accurately capturing modal content information without including excessive communication load and power requirements within the network. Well suited distributed implementations for several local sensor communities sensing only some of the structure's locations could be the solution. The reduced processed data is then gathered from the different locations of the structure and global modal content information can be inferred using the information from the different locations.
- Optimal sensor placement must be considered. There are many issues to consider when deploying a wireless sensor network for a particular application. Effective sensor placement decisions must be driven based on power consumption and communication bandwidth requirements.
- Accurate mode shape estimation is usually conditioned on data measurement with reliable time synchronization protocols. A thorough evaluation regarding the influence of time synchronization and the consequent development of on-board techniques capable of accommodating this constraint must be also performed.

REFERENCES

- Adler, R., Flanigan, M., Huang, J., Kling, R., Kushalnagar, N., Nachman, L., Wan, C.Y., and Yarvis, M. (2005), "Intel mote 2: An advanced platform for demanding sensor network applications". *Proc., 3th Int. Conference on Embedded networked sensor systems*, 298-298.
- Agre, J.R., Clare, L.P., Pottie, G.J., and Romanov, N.P. (1999). "Development platform for self-organizing wireless sensor networks". *Proc., SPIE – Conference on Unattended Ground Sensor Technologies and Applications, Vol. 3713*, 257-268.
- Aoki, S., Fujino, Y., and Abe, M. (2003). "Intelligent bridge maintenance system using MEMS and network technology". *Proc., SPIE – Smart Systems and NDE for Civil Infrastructure, 5057*, 37-42.
- Basheer, M.R., Rao, V. and Derriso, M. (2003). "Self organizing wireless sensor networks for structural health monitoring". *Proc., the 4th Int. Workshop on Structural Health Monitoring, Stanford, CA, 1193-1206*.
- Bernal, D. (2002). "Load vectors for damage localization". *Journal of Engineering Mechanics. 128(1)*, 7-14
- Bult, K., Burstein, A., Chang, D., Dong, M., Fielding, M., Kruglick, E., Ho, J., Lin, F., Lin, T.H., Kaiser, W.J., Mukai, R., Nelson, P., Newburg, F.L., Pister, K.S.J., Pottie, G., Sanchez, H., Stafsuud, O.M., Tan, K.B., Ward, C.M., Yung, G., Xue, S., Marcy, H. and Yao, J. (1996). "Wireless integrated microsensors". *Technical Digest of the 1996 Solid State Sensor and Actuator Workshop, Transducer Research Foundation, Hilton Head Island, SC., 205-210*.
- Casciati, F., Casciati, S., Faravelli, L., and Rossi, R. (2004). "Hybrid wireless sensor network". *Proc., SPIE – Smart Structures and Materials: Sensors and Smart Structures Technologies for Civil, Mechanical, and Aerospace Systems, Berkeley, CA., 5391*, 308-313.
- Chintalapudi, K., Paek, J., Gnawali, O., Fu, T., Dantu, K., Caffrey, J., Govindan, R., and Johnson, E. (2006). "Structural damage detection and localization using NetSHM". *Proc., IPSN'06, April 19-21, 2006, Nashville, Tennessee*.
- Clayton, E.H. (2002), "Development of an experimental model for the study of infrastructure preservation", *Proc., the National Conference on Undergraduate Research, Whitewater, Wisconsin*.

Clayton, E.H., Koh, B.H., Xing, G., Fok, C.L., Dyke, S.J. and Lu, C. (2005), "Damage detection and correlation-based localization using wireless Mote sensors", *Proc., '05 The 13th Mediterranean Conference on Control and Automation, Limassol, Cyprus*.

Clayton, E.H., Qian, Y., Orjih, O., Dyke, S.J., Mita, A. and Lu, C. (2006). "Off-the-shelf modal analysis: Structural health monitoring with motes". *Proc., the 24th International Modal Analysis Conference*.

Clayton, E.H. (2006). Frequency correlation-based structural health monitoring with smart wireless sensors. *Master of Science Thesis, Washington University in St. Louis*.

Cooley, J.M. and Tukey, J.W. (1965). "An algorithm for the machine calculation of complex Fourier series". *Mathematics of Computation*. 19:297-301.

Contursi, T., Messina, A., Williams, E.J. (1998). "A multiple-damage location assurance criterion based on natural frequency changes". *Journal of Vibration and Control*. No.4, pp 619-633.

Crosbow Technologies iMote2 Mote IPR2400 (2007)
<http://www.xbow.com/Products/productdetails.aspx?sid=253>

Dust Networks. <<http://www.dust-inc.com>>

Elson, J., Girod, L., and Estrin, D. (2002). "Fine-grained network time synchronization using reference broadcast". *Proc., 5th Symposium on Operating Systems Design and Implementation, Boston, MA*.

Farrar, C.R., Allen, D.W., Ball, S., Masquelier, M.P., and Park, G. (2005). "Coupling sensing hardware with data interrogation software for structural health monitoring". *Proc., 6th International Symposium on Dynamic Problems of Mechanics, Ouro Preto, Brazil*.

Ferzli, N.A., Sandburg, C.J., King, T., Pei, J.S., Zaman, M.M., Refai, H.H, Ivey, R.A., and Harris, O. (2006). "Experimental investigation of 'smart dust' for pavement condition monitoring". *Proc., the 24rd International Modal Analysis Conference (IMAC XXIV), St. Louis, MO, January 30 - February 2, 2006*

Ganeriwal, S., Kumar, R., and Srivastava, M.B. (2003). "Timing-sync protocol for sensor networks". *Proc., 1st International Conference On Embedded Networked Sensor Systems, Los Angeles, CA, 138-149*

Gangone, M.V., Whelan, M.J., Janoyan, K.D, Cross, K., and Jha, R. (2007). "Performance monitoring of a bridge superstructure using a dense wireless sensor network," *Proc., the 6th International Workshop on Structural Health Monitoring, Stanford, California*.

- Gao, Y. (2005). Structural Health Monitoring Strategies for Smart Sensor Networks. *Doctor of Philosophy Thesis, The University of Illinois at Urbana-Champaign.*
- Hackmann, G., Sun, F., Castaneda, N., Lu, C., Dyke, S. (2008). "A holistic approach to decentralized structural damage localization using wireless sensor networks", *Proc., the Real-time Systems Symposium, 2008*
- Hill, J., and Culler, D. (2002). "Mica: A wireless platform for deeply embedded networks". *IEEE Micro.*, 22(6), 12-24.
- Hollar, S. (2000). COTS Dust. *Master's thesis, University of California, Berkeley, CA.*
- Juang, J.N. and Pappa, R.S. (1985). "An eigensystem realization algorithm for modal parameter identification and model reduction". *Journal of Guidance Control and Dynamics.* 8:620-627
- Kawahara, Y., Minami, M., Morikawa, H., and Aoyama, T. (2003). "Design and implementation of a sensor network node for ubiquitous computing environment". *Proc., IEEE Semiannual Vehicular Technology Conference, Orlando, FL., 5, 3005-3009.*
- Kim, S. (2005). Wireless sensor networks for structural health monitoring. *Master's thesis, University of California at Berkeley.*
- Kim, S. (2007). Wireless Sensor Networks for High Fidelity Sampling. *Ph.D. Dissertation, University of California at Berkeley.*
- Kim, S., Pakzad, S., Culler, D., Demmel, J., Fenves, G., Glaser, S., and Turon, M. (2007). "Health monitoring of civil infrastructures using wireless sensor networks". *Proc., the 6th International Conference on Information Processing in Sensor Networks (IPSN '07), Cambridge, MA, April 2007, ACM Press, pp. 254-263.*
- Kiremidjian, A.S., Straser, E.G., Meng, T.H., Law, K. and Soon, H. (1997). "Structural damage monitoring for civil structures". *Proc., Int. Workshop on Structural Health Monitoring, Stanford, CA, 371-382.*
- Kling, R. (2003). "Intel Mote: an enhanced sensor network node". *Proc., Int. Workshop on Advanced Sensors, Structural Health Monitoring, and Smart Structures, Tokyo, Japan.*
- Koh, B.H. and Dyke S. J. (2007). "Structural damage detection in cable-stayed bridges using correlation and sensitivity of modal data". *Computers and Structures. Vol. 85, pp. 117-130*

- Kottapalli, V.A., Kiremidjian, A.S., Lynch, J.P., Carryer, E., Kenny, T.W., Law, K.H., and Lei, Y. (2003). "Two-tiered wireless sensor network architecture for structural health monitoring". *Proc., SPIE – The International Society for optical Engineering – Smart Structures and Materials, 5057, 8-19.*
- Levy, E.C. (1959). "Complex-curve fitting". *IRE Transactions on Automatic Control. Vol. 4, pp. 37-44.*
- Liu, S.C. and Tomizuka, M. (2003). "Strategic research for sensors and smart structures technology". *Proc., the International Conference on Structural Health Monitoring and Intelligent Infrastructure, Tokyo, Japan, November 13-15, Vol.1, 113-117.*
- Liu, S.C. and Tomizuka, M. (2003). "Vision and strategy for sensors and smart structures technology research". *Proc., the 4th International Workshop on Structural Health Monitoring, Stanford, CA, September 15-17, 42-52.*
- Lynch, J.P., Kiremidjian, A.S., Law, K.H., Kenny, T. and Carryer, E. (2002). "Issues in wireless structural damage monitoring technologies", *Proc., the Third World Conference on Structural Control, 2002, Vol.2: 667-672*
- Lynch, J.P., Sundararajan, A., Law, K.H., Kiremidjian, A.S., and Ed Carryer. (2004). "Embedding damage detection algorithms in a wireless sensing unit for operational power efficiency". *Smart Materials and Structures. 2004, 13: 800-810.*
- Lynch, J.P. (2004). "Overview of wireless sensors for real time health monitoring of civil structures". *Proc., the 4th International Workshop on Structural Control, June 2004, pp. 189-194*
- Lynch, J.P., Wang, Y., Law, K.H., Yi, J.-H., Lee, C.G., and Yun, C.B. (2005). "Validation of a large-scale wireless structural monitoring system on the Geumdang bridge". *Proc., the Int. Conference on Safety and Structural Reliability, Rome, Italy.*
- Lynch, J. P. and Loh, K. (2006). "A summary review of wireless sensors and sensor networks for structural health monitoring". *Shock and Vibration Digest. In press*
- Lynch, J. P. (2006). "Design of a wireless active sensing unit for localized structural health monitoring". *Structural Control and Health Monitoring. In press*
- Maroti, M., Kusy, B., Simon, G., and Ledeczki, A. (2004). "The flooding time synchronization protocol". *Proc., 2nd International Conference On Embedded Networked Sensor Systems, Baltimore, MD, 39-49.*
- Mason, A., Yazdi, N., Najafi K., and Wise K. (1995), "A low-power wireless micro-instrumentation system for environmental monitoring". *Proc., 8th Int. Conference on Solid-State Sensors and Actuators, Stockholm, Sweden, 107-110.*

Mechitov, K.A., Kim, W., Agha, G.A., and Nagayama, T. (2004). "High-frequency distributed sensing for structure monitoring". *Proc., 1st Int. Workshop on Networked Sensing Systems, Tokyo, Japan, 101-105.*

Messina, A., Jones, I.A. and Williams, E.J. (1996). "Damage detection and localization using natural frequencies changes". *Proc., Conference on Identification in Engineering Systems, Swansea, U.K., pp 67-76.*

Messina, A., Williams, E.J., Contursi, T. (1998). "Structural damage detection by a sensitivity and statistical-based method". *Journal of Sound and Vibration. Vol 216, No 5, pp. 791-808.*

MicroStrain Inc. <<http://www.microstrain.com>>

Millennial Net. <<http://www.millennial.net>>

Nagayama, T., Rice, J.A. and Spencer, B.F. Jr. (2006), "Efficacy of Intel's Imote2 wireless sensor platform for structural health monitoring applications". *Proc., Asia-Pacific Workshop on Structural health Monitoring, Yokohama, Japan.*

Nagayama, T. (2007). Structural health Monitoring using smart sensors. *Doctor of Philosophy Thesis, The University of Illinois at Urbana-Champaign.*

Pakzad, S.N., Kim, S., Fenves, G.L., Glaser, S.D., Culler, D.E. and Demmel, J.W. (2005). "Multi-purpose wireless accelerometers for civil infrastructure monitoring", *Proc., the 5th International Workshop on Structural Health Monitoring (IWSHM 2005), Stanford, CA.*

Pei, J.S., Ivey, R.A., Lin, H., Landrum, A.R., Sandburg, C.J., Ferzli, N.A., King, T., Zaman, M.M., Refai, H.H. and Mai, E.C. (2008). "An experimental investigation of applying Mica2 motes in pavement condition monitoring", *Journal of Intelligent Material Systems and Structures. Vol 00 - 2008*

Rice, J.A., Mechitov, K.A., Spencer, Jr., B.F., and Agha G.A. (2008). "A service-oriented architecture for structural health monitoring using smart sensors", *Proc., the 14th World Conference on Earthquake Engineering, Beijing, China*

Sazonov, E., Janoyan, K., Jha, R. (2004). "Wireless intelligent sensor network for autonomous structural health monitoring". *Proc., SPIE – Smart Structures and Materials: Smart Sensor Technology and Measurement Systems, 5384, 305-314.*

Sensametrics. <<http://www.sensametrics.com>>

Sensicast Systems. <<http://www.sensicast.net>>

Shinozuka, M. (2003). "Homeland security and safety". *Proc., Structural Health Monitoring and Intelligent Infrastructure, Tokyo, Japan, 1139-1145.*

Sohn, H., Farrar, C.R., Hemez, F.M., Shunk, D.D., Stinemates, D.W. and Nadler, B.R. (2004). "A review of structural health monitoring literature from 1996–2001". *Los Alamos National Laboratory report LA-13976-MS.*

Spencer, Jr., B.F. (2003). "Opportunities and challenges for smart sensing technology". *First International Conference on Structural Health Monitoring and Intelligent Infrastructure, Tokyo, 13-15 November 2003.*

Spencer, Jr., B.F. and Nagayama, T. (2006). "Smart sensor technology: a new paradigm for structural health monitoring". *Proc., Asia-Pacific Workshop on Structural health Monitoring, Yokohama, Japan.*

STMicroelectronics. (2005), LIS3L02DQ data Sheet
<http://www.st.com/stonline/products/literature/od/10175/lis3l02dq.pdf>

Straser, E.G. and Kiremidjian A.S. (1996). "A modular visual approach to damage monitoring for civil structures". *Proc., SPIE – Smart Structures and Materials, San Diego, CA, 2719, 112-122.*

Straser, E.G. and Kiremidjian A.S. (1998). "A modular, wireless damage monitoring system for structures". *The John A. Blume Earthquake Engineering Center Technical Report. 128.*

The Illinois SHM Services Toolkit. (2008) : <http://shm.cs.uiuc.edu/software.html>

The MathWorks. (2007): <http://www.mathworks.com/>

TinyOS: <http://www.tinyos.net/>

Wang, M.L., Gu, H., Lloyd, G.M., and Zhao, Y. (2003). "A multi-channel wireless PVDF displacement sensor for structural monitoring." *Proc., Int. Workshop on Advanced Sensors, Structural Health Monitoring and smart Structures, Tokyo, Japan, 1-6.*

Vita

Nestor E. Castaneda

Date of Birth	March 09, 1978
Place of Birth	Lima, Peru
Degrees	B.S. Civil Engineering, July 2004 M.S. Civil Engineering, December 2008
Professional Societies	Chi Epsilon – Civil Engineering Honor Society Earthquake Engineering Research Institute
Publications	<p>Castaneda, N., Dyke, S., Lu, C., Sun, F., Hackmann, G. (2008). “Experimental Deployment and Validation of a Distributed SHM System Using Wireless Sensor Networks”, <i>Structural Engineering & Mechanics</i>. (under review)</p> <p>Castaneda, N., Sun, F., Dyke, S., Lu, C., Hope, A., Nagayama, T., (2008). “Implementation of a Correlation-based Decentralized Damage Detection Method Using Wireless Sensors”, <i>Proceedings of the 2008 ASEM Conference, Jeju, Korea</i>.</p> <p>Castaneda, N., Sun, F., Dyke, S., Lu, C., Hope, A., Nagayama, T., “Experimental validation of a correlation-based damage detection technique using imote2 wireless sensors”. (2008). <i>The fifth international workshop on structural control and monitoring, Harbin, China</i></p> <p>Hackmann, G., Sun, F., Castaneda, N., Lu, C., and Dyke, S., (2008). "A Holistic Approach to Decentralized Structural Damage Localization Using Wireless Sensor Networks," <i>Proceedings of 29th IEEE Real-Time Systems Symposium (RTSS 2008)</i></p> <p>Hackmann, G., Sun, F., Castaneda, N., Lu, C., and Dyke, S., "A Holistic Approach to Decentralized Structural Damage Localization Using Wireless Sensor Networks," <i>IEEE Transactions on Parallel and Distributed Systems</i> (under review).</p>

Dyke, S., Castaneda, N., Moore, M., So, M. (2007), "Virtual Experiments for Teaching Hysteretic Structural Behavior", *Proceedings of the 2007 ICEER Conference, Melbourne, Australia.*

December 2008

Short Title: Distributed SHM Using Wireless Sensors

Castaneda, M.S. 2008